T.C.
ABANT IZZET BAYSAL UNIVERSITY
THE GRADUATE SCHOOL OF NATURAL AND APPLIED SCIENCES

OBTAINING A PROFILE OF TAU NEUTRINO COMING WITH LARGE ZENITH ANGLE ON AN INCLINED PLANE AND RELATING ITS ENERGY WITH DENSITY OF PARTICLES

MASTER OF SCIENCE

KAAN YÜKSEL OYULMAZ

BOLU, MARCH 2017

T.C.
ABANT IZZET BAYSAL UNIVERSITY
THE GRADUATE SCHOOL OF NATURAL AND APPLIED SCIENCES
THE DEPARTMENT OF PHYSICS

OBTAINING A PROFILE OF TAU NEUTRINO COMING WITH LARGE ZENITH ANGLE ON AN INCLINED PLANE AND RELATING ITS ENERGY WITH DENSITY OF PARTICLES

MASTER OF SCIENCE

KAAN YÜKSEL OYULMAZ

BOLU, MARCH 2017

APPROVAL OF THE THESIS

OBTAINING A PROFILE OF TAU NEUTRINO COMING WITH LARGE ZENITH ANGLE ON AN INCLINED PLANE AND RELATING ITS ENERGY WITH DENSITY OF PARTICLES submitted by **KAAN YÜKSEL OYULMAZ** in partial fulfillment of the requirements for the degree of Master in the Department of Physics, Abant Izzet Baysal University by,

Examining Committee	**Members Signature**
Supervisor Prof. Dr. Haluk DENİZLİ	....
Member Assoc. Prof. Dr. Abdülkadir ŞENOL Abant İzzet Baysal University	....
Member Asist. Prof. Dr. Ali YILMAZ Abant İzzet Baysal University	....

March 27, 2017

....

Prof. Dr. Duran KARAKAŞ

Director, Graduate School of Natural and Applied Sciences

To My Family

DECLARATION

I hereby declare that all information in this document has been obtained and presented in accordance with academic rules and ethical conduct. I also declare that, as required by these rules and conduct, I have fully cited and referenced all material and results that are not original to this work.

KAAN YÜKSEL OYULMAZ

ABSTRACT

OBTAINING A PROFILE OF TAU NEUTRINO COMING WITH LARGE ZENITH ANGLE ON AN INCLINED PLANE AND RELATING ITS ENERGY WITH DENSITY OF PARTICLES
MSC THESIS
KAAN YÜKSEL OYULMAZ
ABANT IZZET BAYSAL UNIVERSITY GRADUATE SCHOOL OF NATURAL AND APPLIED SCIENCES
DEPARTMENT OF PHYSICS
(SUPERVISOR: PROF. DR. HALUK DENİZLİ)
BOLU, MARCH 2017

Cosmic rays hold an important part of astropartical physics. Researches and experiments show that these particles act like shower when they enter the Earth's atmosphere. Not only chemical composition of these particles still deeply under the investigation, but also energies of these particles are research subject. These researches and experiments are revealed that neutrino particles that are neutral particles and have very small mass. These particles initiate showers, especially tau neutrinos, if they interact with the Earth's crust and these kind of showers can be detectable by using Earth Skimming strategy.

This thesis is based on detection strategy of tau neutrino induced showers. Tau neutrino showers were produced on inclined plane according to different energies (10^7 GeV, $5x10^7$ GeV 10^8 GeV, $5x10^8$ GeV and 10^9 GeV), decay mode of tau (π^-, $\pi^- \pi^0$, $\pi^- \pi^0 \pi^0$ and $\pi^- \pi^- \pi^+$) and decay lengths (3 km, 5 km, 7 km and 10 km) with CORSIKA program. Firstly, products of tau neutrino induced showers by CORSIKA program are analyzed and differences between shower energy, decay mode and decay length are represented. Then, products of tau neutrino induced showers are analyzed again with logically placed array of detectors on inclined plane considering Earth Skimmig strategy. As a result of detected particles by detectors, profile of tau neutrino induced showers try to be unveiled by comparing energy, decay mode and decay length. Results of analysis are presented that tau neutrino induced showers can be distinguishable by using Earth Skimming strategy.

Keywords: Cosmic Rays, Astroparticle Physics, Monte Carlo, CORSIKA Program, Extensive Air Showers, Neutrino Astronomy, Ground Based Array

ÖZET

GENİŞ AÇIYLA EĞİMLİ DÜZLEME GELEN TAU NÖTRİNONUN PROFİLİNİN ELDE EDİLMESİ VE ENERJİSİNİN PARÇACIK YOĞUNLUKLARIYLA İLİŞKİSİ
YÜKSEK LISANS TEZI
KAAN YÜKSEL OYULMAZ
ABANT İZZET BAYSAL ÜNİVERSİTESİ FEN BİLİMLERİ ENSTİTÜSÜ
FIZIK ANABILIM DALI
(TEZ DANIŞMANI: PROF. DR. HALUK DENİZLİ)
BOLU, OCAK - 2015

Kozmik ışınlar, astroparçacık fiziğinde önemli bir yer tutmaktadır. Araştırmalar ve deneyler, bu parçacıkların dünyanın atmosferine girdiklerinde sağanak şeklinde davrandıklarını göstermiştir. Bu parçacıklar sadece kimyasal yapıları itibariyle derin bir araştırma altında değildir, aynı zamanda parçacıkların enerjileri de araştırma konusudur. Araştırmalar ve deneyler, nötr ve çok küçük kütleye sahip olan nötrino parçacıkların da diğer parçacıklar gibi davrandığını ortaya çıkarmıştır. Eğer bu parçacıklar dünyanın kabuğuyla etkileşirlerse, özellikle tau nötrino parçacıkları, parçacık sağanaklarını başlatırlar ve bu tür sağanaklar yüzey tarama stratejisiyle belirlenebilir.

Bu tez tau nötrino tetiklemesiyle oluşan sağanakları ve oluşan sağanakların yüzey tarama stratejisiyle tespitini temel almıştır. CORSIKA programı kullanılarak tau nötrino sağanakları farklı enerji (10^7 GeV, $5x10^7$ GeV 10^8 GeV, $5x10^8$ GeV ve 10^9 GeV), bozunum modu (π^-, $\pi^-\ \pi^0$, $\pi^-\ \pi^0\ \pi^0$ ve $\pi^-\ \pi^-\ \pi^+$) ve bozunum uzunluğuna (3 km, 5 km, 7 km ve 10 km) göre eğilimli bir yüzeye üretilmiştir. Öncelikle tau nötrino tetiklemesiyle CORSIKA programı tarafından oluşturulan sağanakların ürünleri analiz edilip, enerji, bozunum modu ve bozunum uzunluklarına göre farklılıkları gösterilmiştir. Daha sonra tau nötrino tetiklemesiyle oluşan sağanakların ürünleri mantıksal olarak oluşturulan algıç dizilimiyle yüzey tarama stratejisi göz önünde bulundurarak tekrar analiz edilmiştir. Yapılan bu analizin sonunda algıçlar tarafından tespit edilen parçacıklar, tau nötrino tetiklemesiyle oluşan sağanaklarının profili enerji, bozunum modu ve bozunum uzunluğu bakımından ortaya çıkarılmaya çalışılmıştır. Yapılan çalışmanın sonunda tau nötrino tetiklemesiyle oluşan sağanaklarının yüzey taraması stratejisiyle ayırt edilebileceği göstermiştir.

Anahtar Kelimeler: Kozmik Işınlar, Astroparçacık Fiziği, Monte Carlo, CORSIKA Programı, Geniş Hava Sağanakları, Nötrino Astronomi, Yeryüzü Tabanlı Dizilim

TABLE OF CONTENTS

LIST OF FIGURES

Page

LIST OF TABLES

Page

LIST OF ABBREVIATIONS AND SYMBOLS

CR : Cosmic Ray

UHECRs : Ultra High Energy Cosmic Rays

GZK-cutoff : K. Graisen, G. Zapsepin and V. Kuzmin cutoff

EAS : Extensive Air Shower

SNRs : Supernova Remnants

PWNe : Pulsar Wind Nebulae

AGN : Active Galactic Nuclei

GRBs : Gamma Ray Bursts

NC : Neutral Current interactions

CC : Charged Current interactions

DOMs : Digital Optical Modules

PMTs : Photomultiplier Tubes

CORSIKA : COsmic Ray SImulations for Kascade

TAUOLA : Monte Carlo for Tau Decays

ACKNOWLEDGEMENTS

I would like to express appreciation to my supervisor, Prof. Dr. Haluk Denizli, always trust and help me with his guidance and moral support to finish my research. I also thank him for tolerance and kindness.

I would like to thanks my friends who are Ozan Kaan Sadıklar, Eren Erdemir and Gani Çağlar Çoban for their friendships and supports.

I would like to special thanks my friends who Umut Keskin, Sinan Öztel and Ümit Hasan Gözkonan for their friendships, supports and suggestions.

I would like to express sincere appreciation to my girlfriend, Gözde Çolak, for her love, trust and invaluable supports.

The author also would like to thank The Scientific and Technological Research Council of Turkey (TUBITAK) for supporting this work under the project number 114F138.

I am grateful to my family for their support, patiance and financial support from begining to end.

1.INTRODUCTION

In the introduction part of this thesis, not only general information about cosmic rays will be detailed but also the source of high energy neutrinos and detection methods of them via ongoing experiments will be discussed. Moreover, earth skimming strategy is described comprehesively.

1.1 History of Cosmic Ray Study

In 1909, Wulf developed electroscope which is a device to measure electrical charge or electrical potential difference. With his electroscope he tried to measure radiation levels at different altitudes. After all, he determined radiation levels change with altitudes and published his work in “Physikalische Zeitschrift”, but it was not accepted widely. However, in 1912, Hess who is considered the father of Cosmic Ray physics made a great observation with enhanced electroscopes in balloon flight. In his balloon flight, he measured radiation level from ground to 5300 meters altitude. Observation results showed radiation levels increased with the altitude. Moreover, his results were confirmed by Kolhörster. Hess received the Nobel Prize in Physics in 1936 for his discovery of cosmic radiation.

Although Millikan known with his famous oil-drop experiment, he also made measurements of ionization due to cosmic rays and he entitled this ionization as “cosmic rays”. Because of the fact that he believed that primary particles which come from outer space to Earth atmosphere were gamma rays or energetic photons.

In 1930, independent experiments were made and cosmic ray intensity measured. According to these results, Rossi provided that most of primitives are positive because of geomagnetic field. Between 1930 and 1945, a plenty of observation were made and investigations confirmed that the primary cosmic rays are mostly protons. However, secondary particles are photons, electrons and muons.

In 1938, Auger and Maze placed detectors with 20 meters distance (Auger et al, 1939). They first measured time coincidence of cosmic rays and observed particles where secondaries originating from a common source. They concluded that cosmic ray particles interact with air in the atmosphere and this initiate a cascade of secondary interactions. A large amount secondary interactions produce a shower of electrons, photons and muons. The additional achievement of this observation was energy of primary particle and obtained by using number of particles as well as energy loss in the atmosphere. As a result of his observation, extensive air showers was discovered.

Nowadays, cosmic rays spectrum is scanned thoroughly by experiments. According to experiments, cosmic rays with lower energies consist of approximately 90% protons , 9 % alpha particles , 1% of heavier ionized nuclei and very small amount positrons and antimatter. Yet, cosmic rays with higher energies which are called Ultra High Energy Cosmic Rays hold some unclear parts to be lighten and observation need array of detectors. As a result of this, it leads to financial and experimental challenge for research as well as researchers.

1.2 Energy Spectrum of Cosmic Rays

Cosmic ray flux have been determined by various important experiments for decades. Results of these experiments showed that the energy range of cosmic rays can be sorted from less than 10^6 eV to more than 10^{20} eV. The energy of cosmic rays obey a power law spectrum, J(E) α $E^{-\gamma}$;

$$J(E) = \frac{dn}{dt dA d\Omega dE} \; \alpha \; E^{-\gamma} \qquad (1.1)$$

where cosmic ray differential flux J depends on the number of cosmic rays n, per area A, time t, solid angle **Ω** , kinetic energy per nucleus E and spectral index γ.

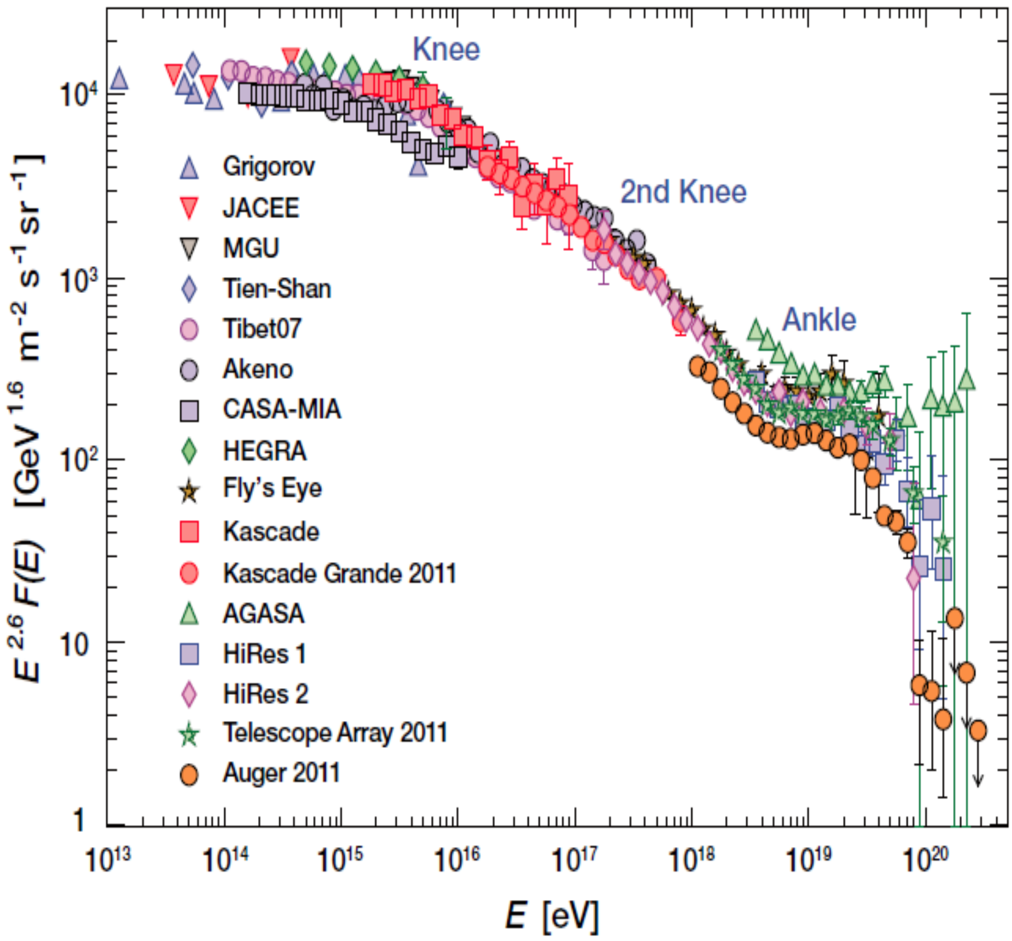

Figure 1.1. The flux spectrum of cosmic rays from air showers. The flux is multiplied by a factor $E^{2.6}$ to make the features known as knee, second knee and ankle better visible. The spectrum follows a power law with changing spectral index γ from 2.7 to 3 (Dova, 2013).

As shown in Figure 1.1, *knee* at an energy about $5x10^{15}$ eV , the spectral index changes from 2.7 to 3.1 (Bluemer et al.,2009). Due to rigidity which is characterized by the ratio of momentum of a cosmic ray particle to its electrical charge, two explanatory approaches exist. First approach assumes an upper acceleration process of the galactic sources. Another one foresees a weak galactic magnetic field which is nearly 0.3 nT. Therefore, a weak galactic magnetic field cannot bend these cosmic particles and this leakage transform smooth slope into sharp slope.

In the *second knee* of an cosmic ray spectrum, spectral index decreases to 2.6 and energy about $4x10^{17}$ eV. Since heavy elements with higher charge escape later according to rigidity formula, second knee predicted as a result of extragalactic sources. Hence, the cosmic ray spectrum gets slightly steeper (Fakenburg and Rhode, 2012).

At the position of the *ankle*, spectral index return to 2.7 with the energy of $3x10^{18}$ eV. A common explanation suggest that extragalactic acceleration becomes dominating process which causes a flatten distribution in the cosmic ray spectrum (Zatsepin and Kuz'min, 1966).

End of the spectrum represents as a cutoff which is a hard to measure due to low flux rate. Moreover, this region is known as "Ultra High Energy Cosmic Rays". In 1966, Graisen, Zapsepin and Kuzmin predicted a cutoff which is also known as GZK-cutoff (Greisen, 1966) that can be act at the end of cosmic ray spectrum. If ultra high energy protons interact with photons of the cosmic microwave background (γ_{CMB}), a short-lived Δ^+ come in sight and Δ^+ resonance is produced which subsequently decays into a lower energetic proton or neutron and neutral pion π^0 or charged pion π^+;

$$p + \gamma_{CMB} \rightarrow \Delta^+ \rightarrow p + \pi^0 \tag{1.2}$$

$$p + \gamma_{CMB} \rightarrow \Delta^+ \rightarrow n + \pi^+ \tag{1.3}$$

Due to photodisintegration, heavier nuclei are split up. In the wake of propagation, high energy incident particle lose energy and cutoff energy is nearly 10^{20} eV. Supernovae and Active Galactic Nucleus are possible source of them. Their distances are nearly 108 light years, 100 Mpc from Earth (Ulrich et al., 2004).

1.3 Extensive Air Showers

Atmosphere of the Earth consists of N_2, O_2 , Ar and other gases. Once primary cosmic ray enters the atmosphere of the Earth, it confronts with gas molecules and interacts with them. As a result of this interactions, hadronic particles (mostly π^-, π^+, π^0, K^+, K^-, K^0) are produced. Moreover, hadronic particles, coming from primary cosmic ray, generate secondaries by interacting gas molecules or decay to other particles. Thus, this immense growth of secondaries is known as Extensive Air Shower (EAS). Secondaries are not only created by hadronic, but also by electromagnetic interactions. However, dominant decay modes of mesons responsible for the generation of the muonic and electromagnetic component of extensive air showers. Therefore, EAS consist of electromagnetic, hadronic and muonic components, see Figure 1.2. Using these distinguish components of EAS, finding and defining primary particle becomes easier.

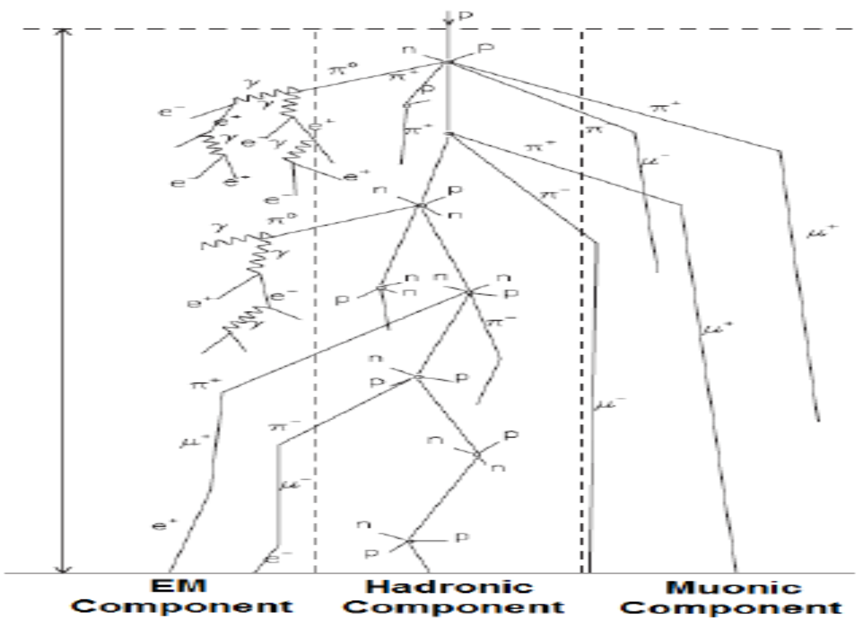

Figure 1.2. Schematic diagram of extensive air shower with electromagnetic component, hadronic component and muonic component (Kapdor-Kleingrothaus, 1997)

1.3.1 Hadronic Component

As mentioned previously, products of the collision which occurs primary particle (proton) with atmospheric nuclei initiates hadronic cascade. Result of this hadronic cascade, secondary particles which are pions, kaons, protons and neutrinos are produced. Then, these secondaries interact with an air molecules again and create new hadrons. Moreover, the charged pions and hadrons decay into muons, whereas the neutral pions decay into photons which starts electromagnetic cascade.

1.3.1.1 Heitler Model for Hadronic Showers

As mentioned before, EAS can initiate by proton, electron or gamma ray. If EAS initiate by a proton, hadronic interaction starts in the atmosphere, producing charged pions and neutral pions. Neutral pions decays into photons and initiate electromagnetic cascade. However, charged pions go on interaction till critical energy of charged pions E_c^{π} . Once they reach critical energy, they decay into muons. According to this informations, Heitler's Model can be modifed and use to approach for EAS which initiated by hadrons.

As shown in Figure 1.3, EAS initiates by a proton. After that, two charged pions, N_{ch}, and one neutral pion $\frac{1}{2} N_{ch}$ are produced. Number of total pions N_{tot} can find for each interaction point;

$$N_{tot} = N_{ch} + \frac{1}{2} N_{ch} \tag{1.4}$$

Because of equal division of energy during particle production, total energy of pions E_{π} related with E_0;

$$E_{\pi} = \frac{E_0}{(N_{tot})^n} \tag{1.5}$$

$$E_{\pi} = \frac{E_0}{\left(\frac{3}{2} N_{ch}\right)^n} \tag{1.6}$$

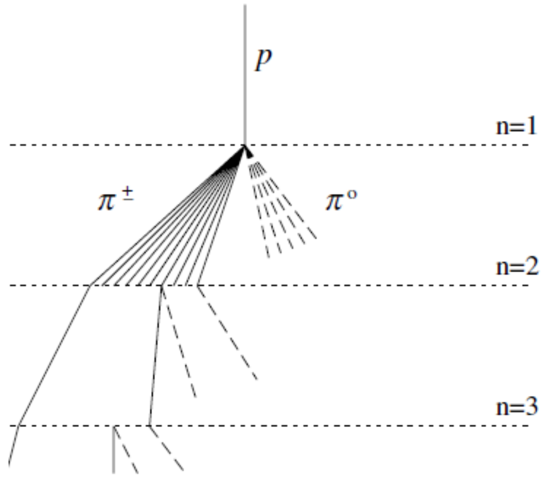

Figure 1.1. Schematic diagram of hadronic cascade with interaction points (Matthews, 2005).

However, this production ends when pions reach or come less than critical energy of pions E_c^{π};

$$E_{\pi} = E_c^{\pi} \tag{1.7}$$

Then, number of interaction point can be derived by using formula;

$$n_c = \frac{\ln\left[\frac{E_0}{E_c^{\pi}}\right]}{\ln\left[\frac{3}{2}N_{ch}\right]} \tag{1.8}$$

As a result of this process, the primary energy is finally divided between pions N_{π} and electrons $N_{e.m}$ partciles in subshower. The number of muons N_{μ} equal to number of pions N_{π} ;

$$N_{\mu} = N_{\pi} \tag{1.9}$$

because of the fact that pions decay into muons. Hence, energy of primary particle which is E_0;

$$E_0 = E_c^{e.m} N_{e.m} + E_c^{\pi} N_{\mu} \qquad (1.10)$$

can calculate energy conservation relation (Matthews, 2005). Therefore, the importance of this model is that E_0 is simply estimated if $N_{e.m}$ and N_{μ} are detected by detectors.

1.3.2 Electromagnetic Component

Neutral pions which are produced from interactions between primary hadronic particle and atmospheric particles decays into photons;

$$\pi^0 \rightarrow \gamma + \gamma \qquad (1.11)$$

$$\pi^0 \rightarrow e^+ e^- + \gamma \qquad (1.12)$$

because of having very short life time $\tau = 8.4 \times 10^{-17}$ seconds.

Products of neutral pions, photons, electrons and positrons, again interact with air nulei N. At higher energies, photons produces electron-positron pairs;

$$\gamma + N \rightarrow e^+ e^- + N \qquad (1.13)$$

which is known pair production and this process continues with Bremsstrahlung;

$$e^{\pm} + N \rightarrow e^{\pm} + \gamma + N \qquad (1.14)$$

The produced Bremsstrahlung photons can produce again electron-positron pairs and this process so on till low energy. At low energies different processes can occur like ionisation, photoelectric effect, Compton effect.

1.3.2.1 Heitler Model for Electromagnetic Showers

Incident particle plays a key role in the structure of an EAS. As mentioned previously, EAS have electromagnetic and hardonic components. Heitler Model describes development of an electromagnetic cascade and bases on the interactions of secondary particles in the cascade as shown in Figure 1.4. Thus, model is not only simple but also it is fundamental for determining structure of EAS. In Heitler model for electromagnetic showers, primary particle can only be electron, positron or photon. Primary particle has a initial energy E_0 and energy splits half of E_0 with new two particle when primary particle interact with a nuclei at the depth X_0 ;

$$E (X) = E_0 / 2^n \qquad (1$$

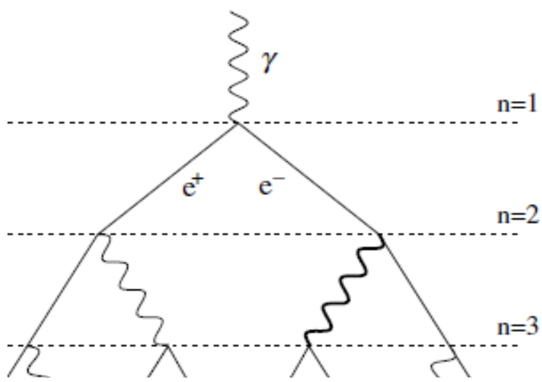

Figure 1.4. Schematic diagram of electromagnetic cascade with interaction points (Matthews, 2005).

However, particles radiates in a length which is λ_e and process goes on with new pair of particles;

$$n = X_0 / \lambda_e \qquad (1.16)$$

At the end of each radiation length new pairs produces and so, particles in the EAS are doubled with formula;

$$N (X) = 2^n \qquad (1.17)$$

Moreover, model can make an assumption about maximum number of particle using critical energy which is approximately $E_c \approx 80$ MeV. If particles reach critical

$$E (X) = E_c \qquad (1.18)$$

energy, particle production end and shower has maximum number of particle;

$$N_{max} (X) = E_0 / E_c \qquad (1.19)$$

Then, maximum atmospheric depth X_{max} can be found approximately (Matthews, 2005).

$$X_{max} \approx \lambda_e \ln(E_0 / E_c) \qquad (1.20)$$

1.3.3 Muonic Component

Hadronic component of the EAS consist of charged pions and kaons. Charged pions and kaons decay into muons;

$$\pi^{+} \rightarrow \mu^{+} + \nu_{\mu} \tag{1.21}$$

$$\pi^{-} \rightarrow \mu^{-} + \bar{\nu}_{\mu} \tag{1.22}$$

$$K^{+} \rightarrow \mu^{+} + \nu_{\mu} \tag{1.23}$$

$$K^{-} \rightarrow \mu^{-} + \bar{\nu}_{\mu} \tag{1.24}$$

$$K^{\pm} \rightarrow \mu^{\pm} + \mu^{0} \tag{1.25}$$

Thus, they are directly related with hardonic component of the EAS and they tell production points in the atmosphere because of limited interactions and scattering in the atmosphere. Produced muons have long lifespan when we compare them electromagnetic and hadronic components of EAS. Also, they spread not much so that they can be important to determine direction of primary particle. As a result of this features of muonic component of EAS, ground based detector systems focus on muonic component of EAS.

1.4 Neutrino and Neutrino Sources

The neutrino is an elementary particle that has no electrical charge and very small mass when it is compared with other elementary particles. As a result of these features, neutrinos are not affected by electromagnetic forces and they are much less affected by gravity. Moreover, they can only interact with matter via the weak nuclear force. Due to fact that neutrinos are not subject to the strong nuclear force, they belong to lepton family. There are three types of neutrinos which are electron neutrino ν_e , muon neutrino ν_μ and tau neutrino ν_τ . All of these types are related with charged leptons which are electron, muon and tau respectively (Griffiths, 2008).

The flux of neutrinos are immense and that means not only neutrinos are on the earth but also they can be found throughout galaxies. The sun just produces a large number of neutrinos like a neutrino factory in the fusion process which is the proton-proton chain reaction. If other stars, cosmic rays and supernova are considered, this abudance of neutrinos cannot seem weird escipecially when their weak interaction feature take into account. However, energies of neutrinos can be different because of sources. Therefore, neutrinos can be divided in two catagories which are low energy and high energ neutrinos. Whereas low energy neutrinos mainly produce in the stars with fusion reactions, high energy neutrinos produces in galactic and extra-galatic sources.

High energy neutrinos have contribution in cosmic ray flux. Thanks to experiments and researches, significance of neutrino flux revealed and understood that where they locate at the cosmic ray spectrum. They locate in a region from knee and above the ankle of the cosmic ray spectrum. Thus, energy of neutrinos can be varied between $\sim 10^{15}$ eV and $\sim 10^{20}$ eV. Most common thought is that high energy neutrino production initiate with proton pairs interaction;

$$p + \gamma \rightarrow \Delta^{+} \rightarrow p + \pi^{0} \quad (2.1)$$

$$p + \gamma \rightarrow \Delta^{+} \rightarrow n + \pi^{+} \quad (2.2)$$

or proton-photon interaction;

$$p + p \rightarrow \Delta^{++} \rightarrow p + p + \pi^{0} \quad (2.3)$$

$$p + p \rightarrow \Delta^{++} \rightarrow p + p + \pi^{+} \quad (2.4)$$

This production creates neutral and charged pions. After that, charged pions decay into muon with a muon neutrio;

$$\pi^{+} \rightarrow \mu^{+} + \nu_{\mu} \tag{2.5}$$

and neutrino production ends when muon decay into electron with a electron neutrino;

$$\mu^{+} \rightarrow e^{+} + \nu_{e} + \overline{\nu_{\mu}} \tag{2.6}$$

Since neutrinos have no charge and very small mass, they play a key role as a messenger for source of cosmic rays and universe. If neutrino can be detected, it gives information about source of neutrino which helps to understand universe and what is happened in universe (Reynolds, 2008)

1.5 High Energy Neutrino Sources

Energy of neutrino is related with its source. Thus, neutrinos are examined in two group which are galactic neutrinos and extra-galactic neutrinos with respect to their sources. In this section, they will be discussed briefly.

1.5.1 Galactic Neutrino Sources

Neutrinos which are produced from galactic sources have at least $3x10^{15}$ eV energy. Due to energy of these neutrinos, they locate in knee region of cosmic ray spectrum. Galactic neutrinos have three main sources which are supernova remnants (SNRs), pulsar wind nebulae and microquars. In this section, they are discussed respectively.

1.5.1.1 Supernova Remnants (SNRs)

A supernova is known as collapse of star basically. However, a star can go supernova in one of two ways. In the first type, a massive star runs out of fuel and some its mass flows into its core. When the core of massive star cannot withstand its own gravitional force, collaption starts with giant explation of a supernova. The second type of supernova occurs in binary star systems. Binary stars are two stars that orbit the same point. If the binary star evolve into white dwarf, one of the star becomes much denser than other star. Because of its dense, gravitional pull initiates and it gather material from second star of the system. When white dwarf reaches maximum level its core becomes immense. Then, runaway reaction ignites and denotes itself in a thermonuclear supernova.

As a result of this explosions, ejected matter expands a high velocities. Moreover, a strong shock wave forms ahead of the ejacta. This process increases particles energy during particle collisions with magnetic clouds in the intersteller medium and cause steady gain in energy. Finally, the shock fronts generate high energy cosmic rays, but these cosmic rays locate at the knee region of cosmic ray spectrum (Yılmaz, 2011).

1.5.1.2 Pulsar Wind Nebulae (PWNe)

As mentioned previously, when massive star collapses supernova explosion occurs and result of this explosion produces SNRs. However, SNRs expands into he interstellar medium. Then, supernova shell is formed and a neutron star may form if collapsed star has immense mass. Neutron star rotates rapidly and it is surrounded by a strong magnetic field. As a result of strong magnetic field and rapid rotation, magnetosphere of pulsar accelerates particles to high energies. This process called a pulsar wind which is magnetized outflow. When the pulsar wind interacts with SNRs, high energy particles emit and these particles are blowed out by inverse Comphoton mechanism. All of these processes inflate a synchrotron-emmiting bubble which is called a pulsar wid nebulae (PWNe) or plerion (Amato, 2014).

1.5.1.3 Microquasars

Microquasar is an X-ray binary system which is powered by spinning black hole or neutron star with a companion star. It has basically three contens which are spinning black hole or neutron star, accretion disk and collimated jets of relativistic particles. Mass of black hole or neutron star can be a few solar masses. Accretion disk has immense angular momentum. As a result of this, disk structure is formed from materials of companion star. Relativistic jets produced with the help of accretion disk and magnetic field. The jets contain relativistic electrons and they outflow two sides of microquasar (Mirabel and Rodriguez, 2014).

1.6.2 Extra-Galactic Neutrino Sources

Ultra high energy neutrinos locates at the ankle of cosmic ray spectrum with energy $\sim 10^{20}$ eV. They have two main sources which are active galactic nuclei and gamma ray burst. These sources are important to understand universe and also cosmic ray physics. In this section, extra-galactic neutrino source are discussed briefly.

1.6.2.1 Active Galactic Nuclei (AGN)

Active galactic nuclei (AGN) is known as the most luminious objects in the universe and it can be found at the center of some galaxies. AGN is powered by supermassive black hole and it is surrounded by a gaseous accretion disk like microquasar. However, AGN has great amount of luminous so that it can differ from microquasar. Thus, it is called quasar which is the most energetic form of AGN. AGN emits in the radio, microwave, infrared, optical, ultra-violet, X-ray and gamma ray wave bands (Swinburne Astronomy Web Site).

1.6.2.2 Gamma Ray Bursts (GRBs)

Gamma ray bursts (GRBs) are the most powerful events in the universe and they are burst of highly energetic gamma rays. Mechanism of GRBs are related with collapse of extraordinary massive star, hypernova, and black hole. When accreted matter from hypernova tunnels into a pair of powerful jets by drilling outter layer of dying star, these burst of jets can be seen as a flash of gamma ray light. However, these flash of gamma rays just take very short time.As a result of process, GRBs produces optical, X-ray and gamma ray wave bands. These powerful events prove highly energetic particles with energy nearly exa electron volt (EeV). Hence, GRBs are commonly seems as not only a sources of the highest energy cosmic rays but also high energy neutrino sources. In brief, GRBs not only tells secrets of universe, but also they show limits of cosmic ray spectrum (NASA Web Site).

1.7 Detection of High Energy Neutrinos

Detection of high energy neutrinos is a tough work, since they have no electrical charge and very small mass. Moreover, they weakly interact with other particles. Although these features of high energy neutrinos make them hard to detect, they can be detected with different detectors such as water Cherenkov detectors, extensive air shower detectors and acoustic detectors by observing interactions of neutrinos.

Neutrinos can interact with a nucleus in two ways which are neutral current (NC) and charged current (CC) interactions. In the neutral current interaction, neutrino ν_l interacts with nucleus N and then the Z^0 boson shows up itself. Afterward, this process ends with neutrino ν_l and hadronic cascade X;

$$\nu_l + N \rightarrow Z^0 \rightarrow \nu_l + X \tag{2.7}$$

On the other hand, neutrino again interacts with nucleus N and this time $W^{\pm}$ boson comes up. Then, lepton *l* is released with haronic cascade X in the weak interaction.

$$\nu_l + N \rightarrow W^{\pm} \rightarrow l + X \qquad (2.8)$$

Under favour of these interaction types, neutrinos can be detected with array of detectors or immense volume detectors. However, these detectors detect interaction product or sub-products of product. This section continues with some important observatories such as Pierre Auger Observatory, IceCube Neutrino Observatory and Super-Kamiokande.

1.7.1 IceCube Neutrino Observatory

The IceCube Neutrino Observatory or IceCube is a neutrino detection observatory which locates at the Sout Pole. IceCube consist of 5,160 digital optical module (DOMs) and ecah one has photomultiplier tubes with its electronics (IceCube Collaboration, 2009). The DOMs are linked strings by 17 meters seperation and each one compose of 60 DOMs. The strings are separated 125 meters from each other with the shape of hexogonal grid. All of strings are buried in the Antartic ice sheet between 1,450 meters and 2,450 meters depth. In addition, detector system can detect all neutrino types with the energy range from 100 GeV to 10^9 GeV. Hence, this features makes it special when it is compared with other ground based cosmic ray detectors. Moreover, IceCube Neutrino Observatory has surface array, IceTop, for cosmic ray observation and it consists of 81 stations which are furnished with DOMs. IceTop detects not only air showers with directions but also measures flux of the location with 300 TeV to 1 EeV energy range (Abbasi et al., 2010a).

IceCube detector system detects neutrinos with the help of charge current interaction of neutrino. When high energy neutrino passing through ice, it makes charge current interaction with an ice. As a result of process, charged secondary particles are produced. Secondary particles emit Cherenkov lights that are products of charged particles if charged particles exceed speed of light in ice. Then, Cherenkov lights are detected from DOMs and signals are sent laboratory to investigate (Abbasi et al, 2010b).

1.7.2 Super-Kamiokande

Super-Kamiokande or Super-K is a large neutrino observatory which is located 1,000 meters underground in the Kamioka-mine, Japan. It consist of stainless-stell tank that is 39.3 meters diameter and 41.4 meters tall. Cylindrical shape of tank is filled with 50,000 tons ultra pure water and inner surface of tank is surrounded by 11,146 photomultiplier tubes (PMTs). Energy range of Super-K can vary between 100 MeV and 100 TeV.

Neutrino detection principle of observatory depends on charge current interaction like in IceCube with detecting Cherenkov lights. However, this time Cherenkov lights produce in ultra pure water. Then, all of Cherenkov lights are detected by PMTs and signals are sent laboratory for research (Fukuda et al., 2003).

1.7.3 Pierre Auger Observatory

The Pierre Auger Observatoy is ground based observatory to detect high energy cosmic rays. Observatory locates in Argentina with surface particle detector array. The surface detector array consists of 1,600 tanks filled with pure water and each tank has photomultiplier tube (PMT) to detect Cherenkov lights which produces from interaction of particles with pure water inside of tank. In the surface particle detector array, tanks are located with 1.5 km spacing. Surface particle detector array detects secondary particles of atmospheric extensive air showers. Then, information particle densities of tanks are gathered and air shower is constracted with energy and direction by using softwares (Pierre Auger Collaboration Web Site).

The Pierre Auger Observatory not only try to determine atmospheric cosmic ray shower but also try to determine neutrino based air shower with the help of surface particle detector array. Observatory is surrounded by mountains and location of observatory helps to detect tau neutrio showers that are produced in the interaciton of tau neutrino with mountains. If tau neutrino intract with moutain, it makes charge current and tau comes up. This procces ends with tau decay into other particles when tau go out from mountain. Moreover, other particles from tau decay makes extensive shower, if tau neutrino is high energy neutrino. Secondary particles of neutrino induced particle shower can detect from surface particle detector array like other extensive air shower. However, neutrino induced showers are very inclined and this makes it hard work according to other extensive air shower. All of this type showers are called neutrino induced downward-going showers (Abreu, 2013).

1.8 Earth-Skimming Strategy

All of neutrino detection experiments take advantages of charge current interaction of neutrinos with special targets such as water, ice etc. Earth skimming strategy is basically neutrino detection method with the help of the Earth's crust as a target. However, this method is plausible to detect high energy tau neutrinos because electron that comes out from electron neutrino makes showers without going out and muon that comes out from muon neutrino travels long distances with small energy loses.

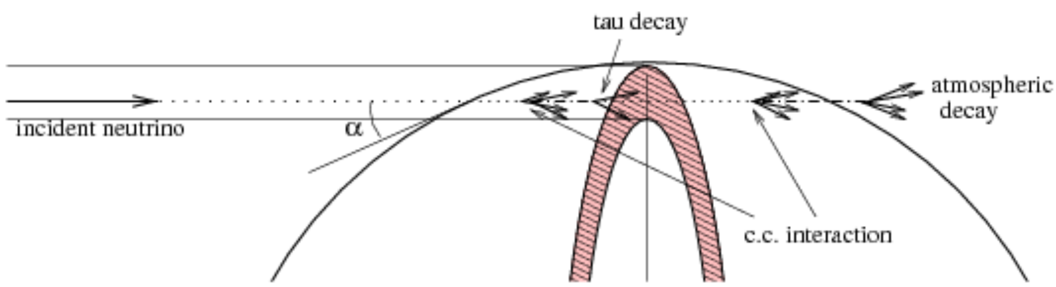

Figure 1.5. Development of tau neutrino induced shower in the Earth's crust (Bigas et al, 2009).

In coming high energy tau neutrino undergoes charged current interaction inside of the Earth's crust and process goes on with tau lepton and hadron shower. Tau lepton goes out from the Earth's crusts and decays into hadrons or electron that produce air shower in atmosphere as shown in Figure 1.5. If produced air shower can be detected by placing array of detector, shower can be contracted and energy of tau lepton can be estimated. However, produced tau lepton need to be nearly horizontal so that produced air shower from hadrons or electron can be detected by detectros. Moreover, tau lepton need to be decay into hadrons or electon when goes out from the Earth's crust or else. Then, hadrons or electron decay into other particles because of high dense (Bigas et al, 2009).

2. AIM AND SCOPE OF THE STUDY

Cosmic rays are high energetic particles which come from space and bombard the Earth's atmosphere. They are the most interesting subject of astrophysics. After discovery of them, scientists tried to understand and unveil this misterious phenomenon. Chemical composition of these particles are determined by important experiments. According to chemical composition of CR's, they are commonly protons, heavy nuclei, gamma particles and other particles. The results of these researches are shown that energy of cosmic rays are much more than thought and they act like as shower especially Ultra High Energy Cosmic Rays (UHECRs) when they enter atmosphere of the Earth. Moreover, UHECRs can be neutrino particles and neutrinos can be produce shower when it interact with the Earths crust. Due to low mass and no charge, these high energetic neutrino particles play a role as messenger for space and give a clue about events which occur in universe. Thus, aim of this thesis understand tau neutrino induced showers and detect these showers with using earth skimming method. In this thesis, research of ultra high energy tau neutrino induced showers will be simulated by CORSIKA program and produced showers will be detailed comprehensively with pre-analysis of these produced showers. Moreover, study of array placement and logical detector will be explained with particle detection strategy of logical detector. After that, the analysis of showers will be made by placing the array and applying the detection strategy. In the last chapter, results of analysis will be discussed and concluded.

3. MATERIALS AND METHODS

3.1 CORSIKA Program (Cosmic Ray Simulations for Kascade)

CORSIKA is a simulation program which relies on Monte Carlo method for extensive air showers that are initiated by high energy cosmic ray particles. Although it was firstly developed for KASCADE experiment in Germany, it has been used widely for other array experiments with updated new versions.

As mentioned in the first chapter, extensive air shower is produced when cosmic ray particle enters athmosphere of the Earth and interacts with air nuclei or decay into secondary particles. The CORSIKA program produces these secondary particles by tracking each one through athmosphere. Then, it gives information of secondary particles such as particle type, energy, location, arrival time etc. on a user defined plane which can be at specific altitude. Moreover, not only primary cosmic ray can be defined as protons, light nuclei up to iron, photons and other particles, but also energy and direction of primary particle can be defined by user. According to type of selected primary cosmic ray, interaction types which depend on several model can be selected by user. There are several models for these interaction types. While the hadronic interaction at high energies is described by *QGSJET* model, at low energies for hadronic interaction is described by *GHEISHA* model in the CORSIKA program. On the other hand, the interactions for photon or electron can be treated by *EGS4* or *NGK* formula. Also, each model can be reconstructed by changing decay energies of secondary particles such as muons and electrons (CORSIKA Web Site).

In short, extensive air shower can be simulated in the CORSIKA program by defining energy, direction, observation level and interaction type of cosmic ray. Then, using output file of simulation program, extensive air showers can be investigated. In this thesis, modified version of CORSIKA-6990 were used to produce neutrino induced extensive air showerss on 30 degree inclined plane for simulation via earth-skimming strategy.

3.2 Production of Tau Neutrino Induced Showers with CORSIKA Program

As mentioned previous chapter, high energy tau neutrino undergoes charged current interaction inside of the Earth's crust and tau lepton produces as a result of this process. Then, tau lepton decays into hadrons or electron while goes out from the Earth's crust, initiating extensive air shower. Therefore, production of tau neutrino induced showers made with respect to this process. In this section, tau neutrino induced showers will be simulated by CORSIKA program.

CORSIKA program cannot simulate all of mentioned process. However, decays of tau lepton are known and these decays can be used for production of tau neutrino induced showers. As seen in Table 3.1, decay modes of tau lepton are shown and four hadronic decay of tau lepton which are π^-, $\pi^- \pi^0$, $\pi^- \pi^- \pi^+$ and $\pi^- \pi^0 \pi^0$, already produced by TAUOLA,were choosen to produce shower by CORSIKA program.

Table 3.1. Decay modes of tau lepton are shown with respect to secondary particles and probability.

Decay Mode	Secondary Particles	Probability
$\tau \rightarrow \mu^- \bar{\nu}_\mu \nu_\tau$	μ^-	17.39%
$\tau \rightarrow e^- \bar{\nu}_e \nu_\tau$	e^-	17.85%
$\tau \rightarrow \pi^- \nu_\tau$	π^-	11.08%
$\tau \rightarrow \pi^- \pi^0 \nu_\tau$	$\pi^-, \pi^0 \rightarrow 2\gamma$	25.37%
$\tau \rightarrow \pi^- \pi^0 \pi^0 \nu_\tau$	$\pi^-, 2\pi^0 \rightarrow 4\gamma$	9.1%
$\tau \rightarrow \pi^- \pi^0 \pi^0 \pi^0 \nu_\tau$	$\pi^-, 3\pi^0 \rightarrow 6\gamma$	1.08%
$\tau \rightarrow \pi^- \pi^- \pi^+ \nu_\tau$	$2\pi^-, \pi^+$	8.98%
$\tau \rightarrow \pi^- \pi^- \pi^+ \pi^0 \nu_\tau$	$2\pi^-, \pi^+, \pi^0 \rightarrow 2\gamma$	4.30%

Then, energies of selected hadronic decay modes of tau lepton were produced by TAUOLA program (Davidson et al, 2010) which simulates decays of tau lepton by computing energies of hadronic products. Thus, energy of tau lepton which are 10^7 GeV, $5x10^7$ GeV, 10^8 GeV, $5x10^8$ GeV and 10^9 GeV were choosen to simulate by TAUOLA program for selected hadronic decays. In Figure 3.1, selected tau lepton mode which is $\pi^- \pi^0$ was produced by 5×10^7 GeV TAUOLA program. As seen in Figure 3.1, total momentum (P_{tot}) and momentum component (P_x, P_y, P_z) is shown respectively for π^- and π^0.

```
2   50000000.
1    8   0.2701182E+07   0.2701182E+07  -0.1100000E-01  -0.1490000E+00
2    7   0.3767586E+08   0.3767586E+08  -0.3800000E+00  -0.3360000E+00
```

Figure 3.1. TAUOLA program output for $\pi^- \pi^0$ decay mode of tau lepton with 5×10^7 GeV is shown in this figure. In the first line, total energy of tau lepton is shown as GeV. In the second line and third line of figure, momentum informations (P_{tot}, P_x, P_y, P_z) of π^- and π^0 are shown respectively as GeV.

In the production of showers, four decay lengths (first interaction point to observation level) which are 3 km, 5 km, 7 km and 10 km were selected to observe shower development and nine showers produced for each energy, decay mode and decay length. According to energy, decay mode and decay length, showers were labeled with run name to avoid confisuion as seen in Table 3.2. In Table 3.2, first column shows decay mode of showers with numbers from 1 to 5, and second column shows decay length with numbers which are 03, 05, 07, 10 for 3 km, 5 km, 7 km and 10 km, respectively. In the third column of Table 3.2 shower energy is represented with numbers which ranges from 1 to 5 for 10^7 GeV, 5×10^7 GeV, 10^8 GeV, 5×10^8 GeV and 10^9 GeV, respectively. Lastly, produced shower numbers which start from 1 to 9 is shown in the fourth column of Table 3.2. For instance, run name of first produced shower by using 5×10^7 GeV shower energy, $\pi^- \pi^0$ decay mode and 7 km decay length is run10721**.** In the following sections, showers will be referred these run names.

Table 3.2. Naming of showers is represented by used numbers with respect to decay mode, decay length, shower energy and shower number.

Decay Mode	Decay Length	Shower Energy	Shower Number
$\pi^- \pi^0 \rightarrow 1$	03→3 km	1→10^7 GeV	From 1 to 9
$\pi^- \pi^- \pi^+ \rightarrow 2$	05→5 km	2→$5x10^7$ GeV	
$\pi^- \pi^0 \pi^0 \rightarrow 3$	07→7 km	3→10^8 GeV	
$\pi^- \rightarrow 4$	10→10 km	4→$5x10^8$ GeV	
		5→10^9 GeV	

After all, according to earth-skimming strategy for tau neutrino induced showers, CORSIKA program were modified. In this modification, "*QGSJET*" mode was choosen for hadronic interactions at high energies and "*GHEISHA*" mode was choosen for interactions at low energies. Also, shower features which are "slant", "curved" and "upward" were selected for reality adaptations. Then, input card of CORSIKA program which helps to shower arrangement was edited. In this arrangment of input card, zenith angle that ranges from "92.0" to "92.5" degree and azimuth angle that ranges from "0.0 to 0.5" degree were set. CORSIKA program traces particles for using these energy cuts and if energy of particle is below energy cut, CORSIKA program does not trace particle for following interactions. Thus, energy cuts of electron-positron particles were set 100 MeV and energy cuts of muon-antimuon particles were setted 50 MeV. Observation of plane was set 30 degree inclination to observe earth-skimming strategy and plane location was modified for all decay lengths with resprect to starting point of shower. As seen in Figure 3.2, these editted informations of showers and other informations are shown with statements. Input card of CORSIKA program was set for each shower in reference to decay modes, shower energy and decay lengths. Then, the shower production was completed and 720 showers were simulated succesfully by CORSIKA program.

```
RUNNR   10721                                                   run number
EVTNR   1                                                       number of first shower event
NSHOW   1                                                       number of showers to generate
INFILE  input_nupipi0_new/nupipi0_5x10to7_1.dat
THETAP  92.   92.5                                              range of zenith angle (degree)
PHIP    0.    0.1                                               range of azimuth angle (degree)
SEED    110721   0   0                                          seed for 1. random number sequence
SEED    210721   0   0                                          seed for 2. random number sequence
SEED    310721   0   0                                          seed for 3. random number sequence
OBSLEV 2250.E2                                                  observation level (in cm)
FIXHEI 1500.E2  2                                               starting level for the shower generation
MAGNET 20.0 42.8                                                magnetic field centr. Europe
HADFLG 0 0 0 0 0 2                                              flags hadr.interact.&fragmentation
ECUTS 0.1 0.1 0.05 0.05                                         energy cuts for particles
MUADDI F                                                        additional info for muons
MUMULT T                                                        muon multiple scattering angle
ELMFLG F T                                                      em. interaction flags (NKG,EGS)
STEPFC 1.0                                                      mult. scattering step length fact.
RADNKG 200.E2                                                   outer radius for NKG lat.dens.distr.
ARRANG 0.                                                       rotation of array to north
LONGI   T   2.   F   F                                          longit.distr. & step size & fit & out
*  THIN 1.000E-06 1.000E+06 0.000E+00
ECTMAP 1.E3                                                     cut on gamma factor for printout
MAXPRT  1                                                       max. number of printed eventsDIRECT
./                                                              output directory
*   INCLIN  -15500.E2 0.E2 1640.E2 -0.5 0. 0.86     X,Y,Z of origin, normal versors 3k
*   INCLIN  -14000.E2 0.E2 1690.E2 -0.5 0. 0.86     X,Y,Z of origin, normal versors 5k
INCLIN  -11500.E2 0.E2 1790.E2 -0.5 0. 0.86              X,Y,Z of origin, normal versors  7k
*   INCLIN  -9000.E2 0.E2 1900.E2 -0.5 0. 0.86      X,Y,Z of origin, normal versors 10k
DATBAS  T                                                       write .dbase file
PAROUT  F F                                                     for horizontal observation level output
USER abant                                                          user
DEBUG F 6 F 1                                                   debug flag and log.unit for out
EXIT
```

Figure 3.2. Input card of run10721 is shown in figure with set values. In right side of input card, set values of run10721 are shown with explanations.

3.3 Pre-Analysis Results of Tau Neutrino Induced Showers

Produced showers by CORSIKA program were analyzed before placement of array. Pre-anaylsis results are showed distribution of particles on inclined plane, effects of decay modes on shower energy, decay length and percentage of particles in showers. Moreover, pre-analysis results were used for further analysis like center of array. In this section pre-analysis results of produced showers by CORSIKA program will be detailed.

In pre-analysis, data files of showers were analyzed and number of particles or particle types such as gamma, electron etc. on inclined plane were obtained. Distiribution of particles on inclined plane is shower in Figure 3.3 and Figure 3.4 for all particles two dimensionally.

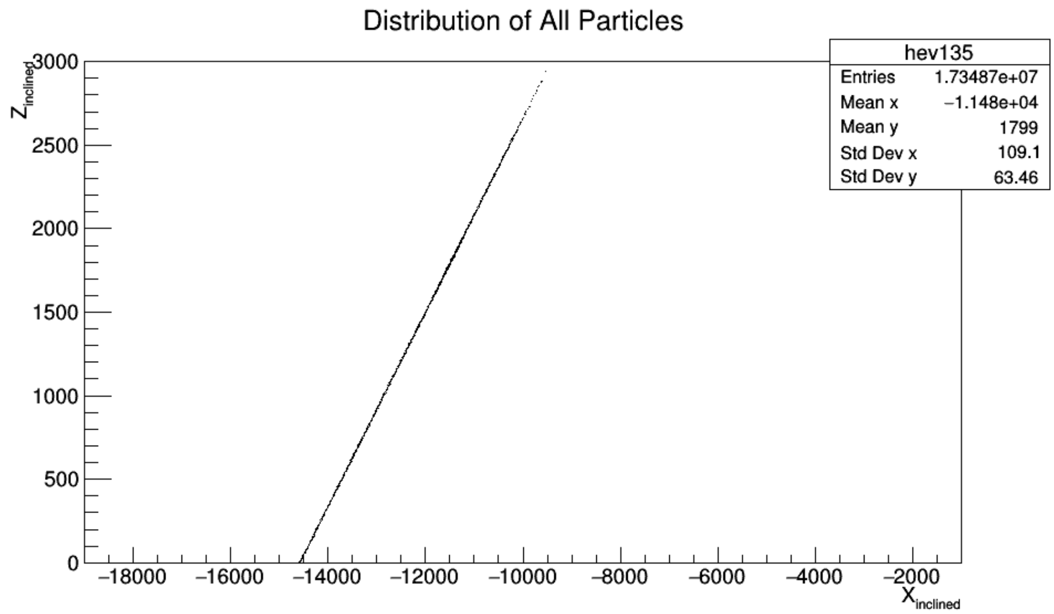

Figure 3.3. Distribution of all particles on inclined plane is shown by using Z versus X frame for run 10721.

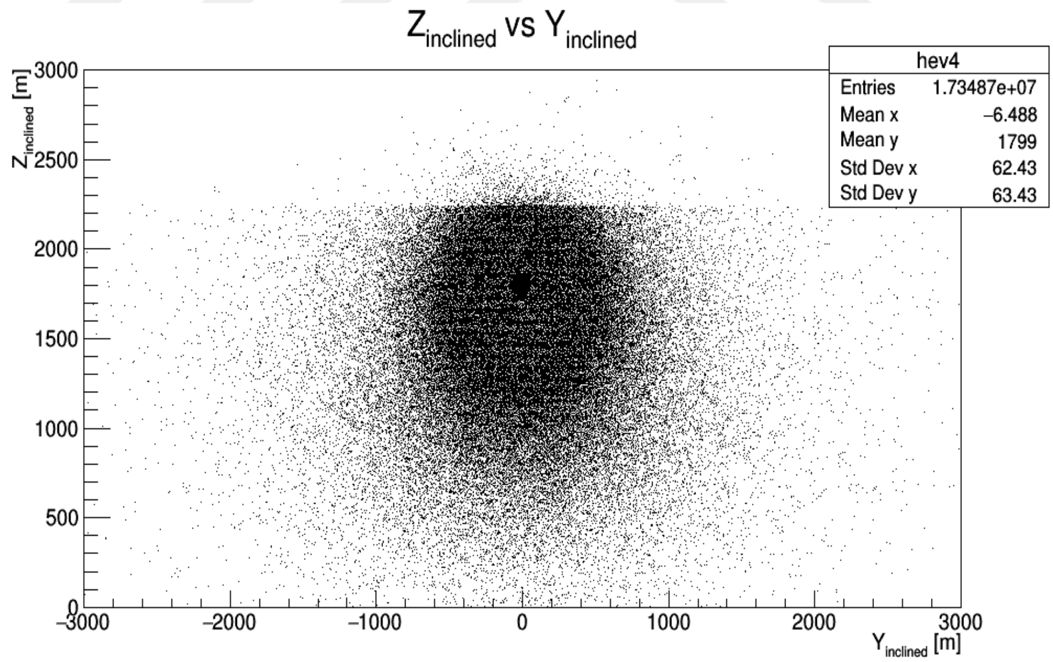

Figure 3.4. Distribution of all particles on inclined plane is shown by using Z versus Y frame for run 10721.

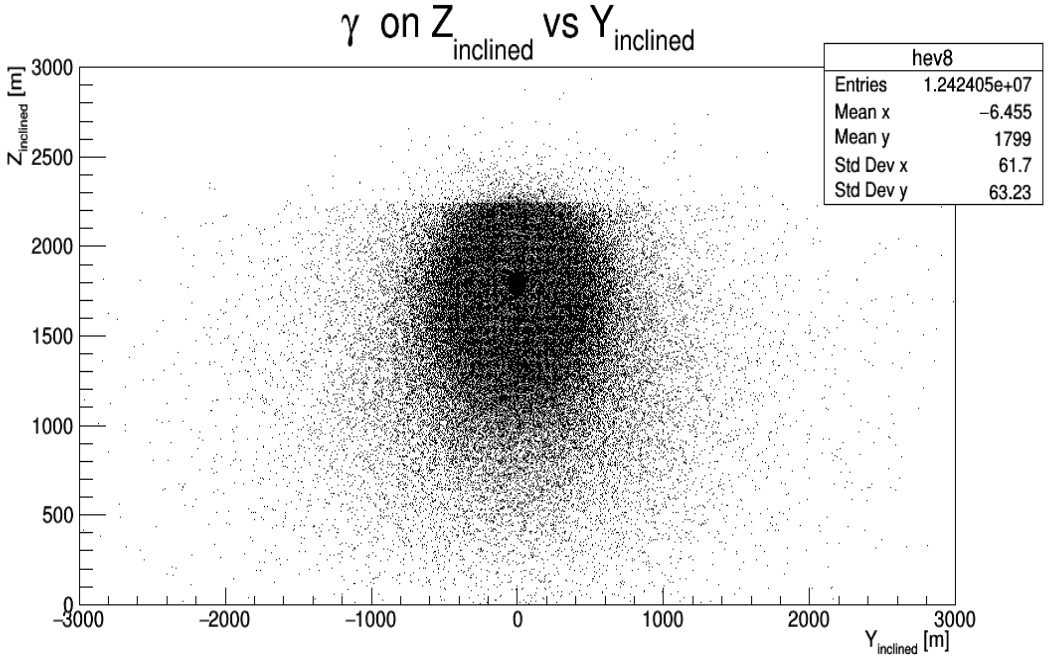

Figure 3.5. Distribution of gamma particles on inclined plane is shown by using Z versus Y frame for run 10721.

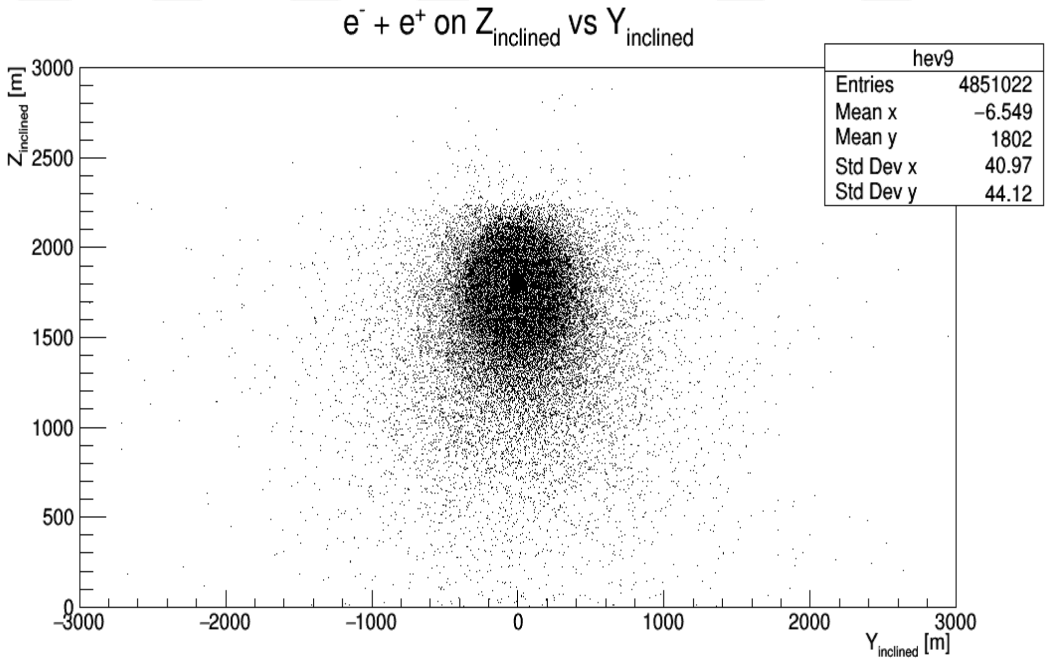

Figure 3.6. Distribution of electron-positron particles on inclined plane is shown by using Z versus Y frame for run 10721.

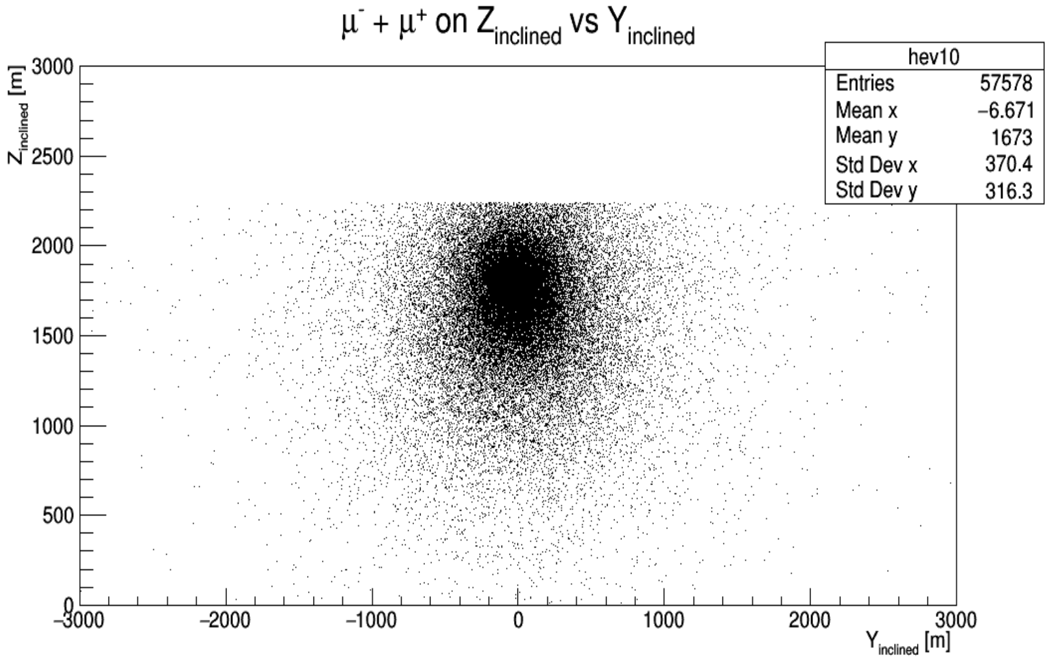

Figure 3.7. Distribution of muon-antimuon particles on inclined plane is shown by using Z versus Y frame for run 10721.

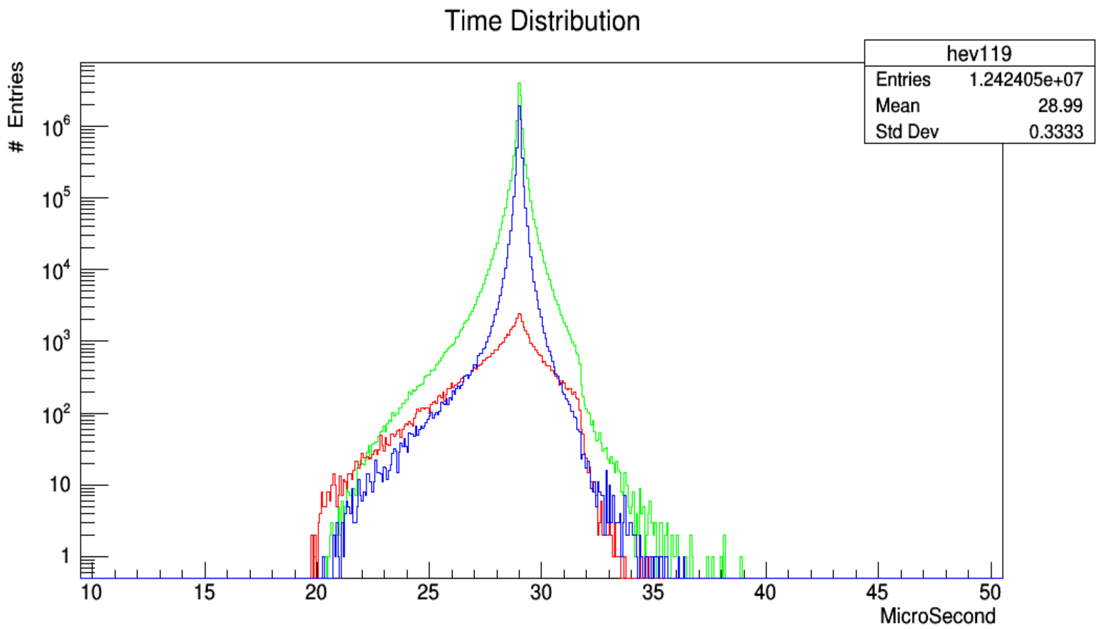

Figure 3.8. In this histogram, time distributions of gamma (green line), electron-positron (blue line) and muon-antimuon (red line) particles on inclined plane are shown for run 10721.

Number of particles by types that are gamma, electron-positron and muon-antimuon are shown also in Figure 3.5, Figure 3.6 and Figure 3.7 respectively. Moreover, distributions of particles on inclined plane were plotted one dimensionally to use placement of array. These graphs show that particle distribution on inclined plane depends on energy cuts which were adjusted in production of showers. As seen in figures, when muon-antimuon and gamma particles are affected, electron-positron particles are not affected these energy cuts. However, this situation is not change center of shower and observation level which is y axis of graphs is enough to place array, since particles on inclined plane distributes mostly center of shower.

Time distribution of particles on inclined plane are shown in Figure 3.8. According to figure, first coming particles are muon-antimuon particles and peak value of time distribution is almost same for all particles.

In Figure 3.9, number of particles on inclined plane obtained without particle distinction for $5x10^7$ GeV $\pi^- \pi^0$ showers by pre-analysis. In accordance with Figure 3.9, increasement of decay length increases particle numbers on inclined plane till 7 km decay length. Then, particle numbers on inclined plane decrease at 10 km decay length with regard to other decay lengths. To generalize all variables of produced tau neutrino induced showers, particle numbers were fitted a function that is f(x) = A and gained mean values of showers with respect to shower energy, decay mode and decay length. Other shower energy, decay modes and decay lengths are presented Appendix A with mean value tables. These mean values were plotted as seen in Figure 3.10. The figure shows that particle numbers on inclined plane are the highest value at 5 km decay length for 10^7, $5x10^7$ and 10^8 GeV in Figure 3.10. However, $5x10^8$ and 10^9 GeV shower energy effect 7 km decay lenght to dominate particle abundance on inclined plane for $\pi^- \pi^0$ and $\pi^- \pi^0 \pi^0$ decay modes. Moreover, energy dependence for particle numbers on inclined plane that escalate with increment of energy can be seen clearly at first glance.

In conclusion, particle numbes on inclined plane show that shower expansion depends on shower energy and decay length. However, decay modes may not be distinct. Thus, ratio of gamma, electron-positron and muon-antimuon may help to determine these decay modes.

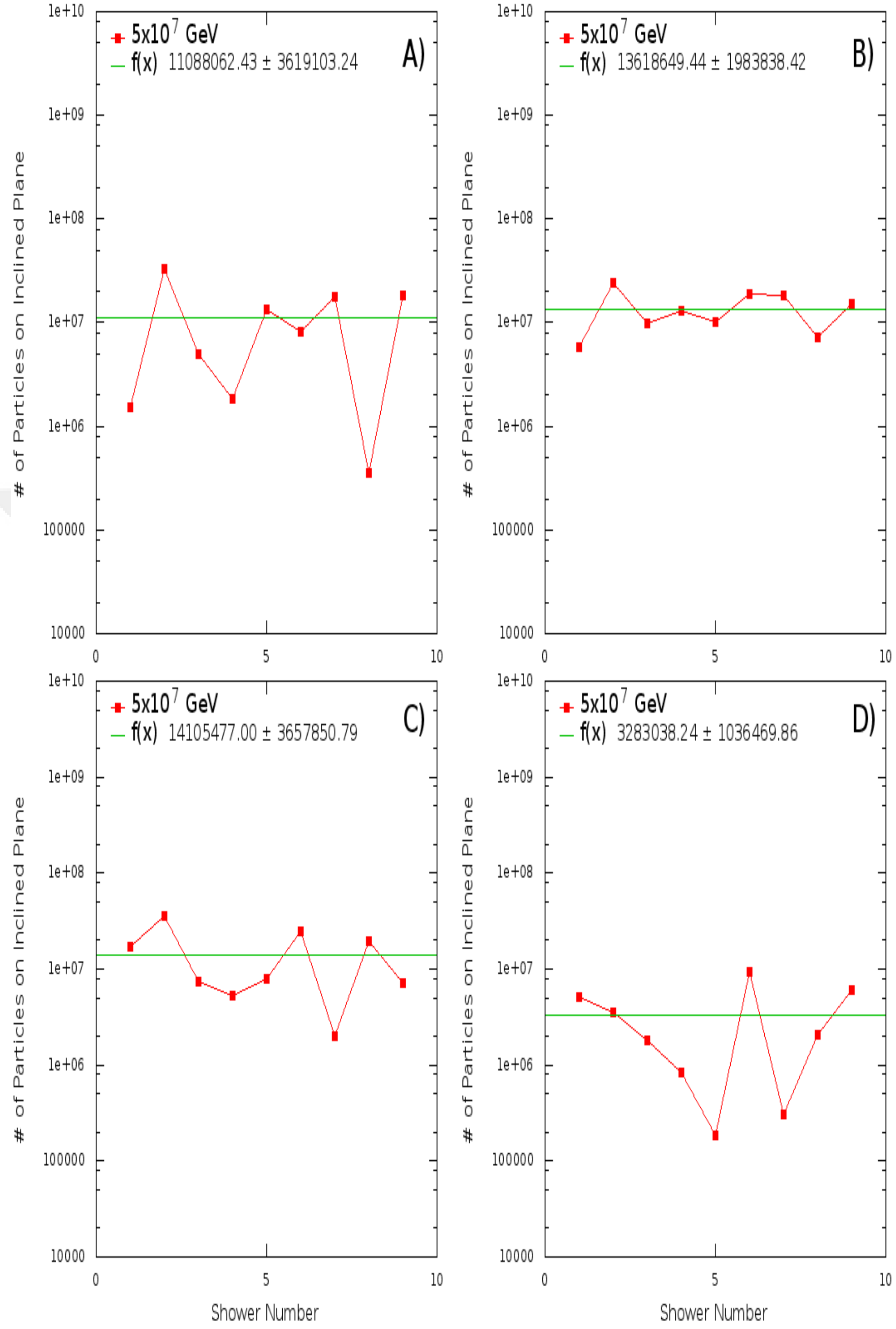

Figure 3.9. Number of particles on inclined plane are shown by using same energy that is 5x10^{7} GeV (red line) and different decay length for nine showers. In A, B, C and D frames of figure, decay length of $\pi^- \pi^0$ showers are 3 km, 5 km, 7 km and 10 km, respectively.

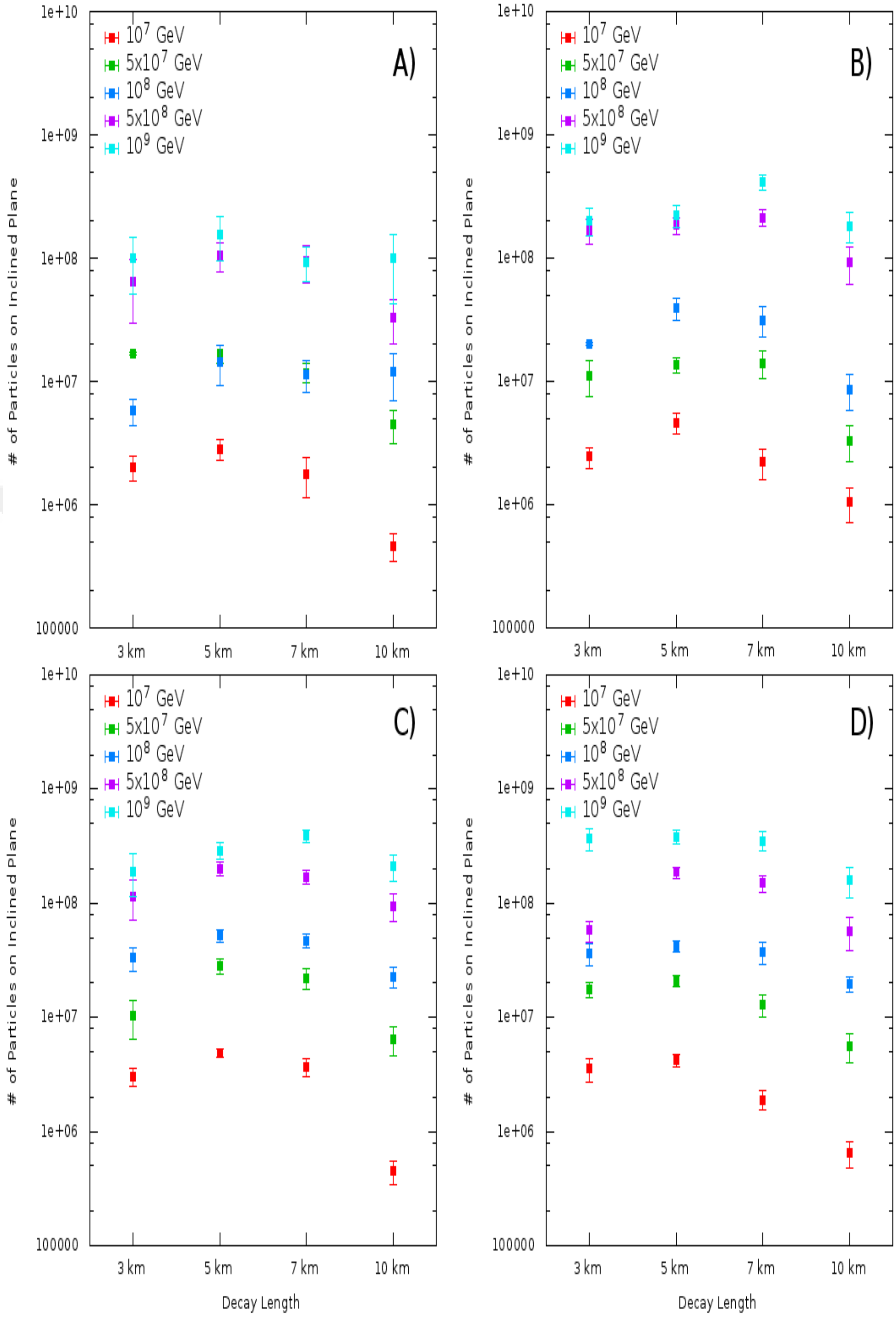

Figure 3.10. Fluctuation on number of particles on inclined plane which is gained by fitting a function for all energies and decay lengths is represented with regard to decay length. π^-, $\pi^-\ \pi^0$, $\pi^-\ \pi^0\ \pi^0$ and $\pi^-\ \pi^-\ \pi^+$ decay modes are shown respectively in A,B,C and D.

According to particle distribution on inclined plane, particle percentages were investigated to find relation between shower energies, decay modes and decay lengths by pre-analysis. In Figure 3.11, particle percentages of showers that were produced $5x10^7$ GeV shower energy and $\pi^- \pi^0$ decay mode are shown and fitted a function to find mean value of percentage for nine showers. In Appendix A, other decay modes and showers energies will be represented with mean value tables.

With the help of these fit values, percentage graphs were plotted by using these fit values. These graphs were plotted separately for particles that gamma, electron-positron and muon-antimuon particles to see differences clearly as seen in Figure 3.12, Figure 3.13 and Figure 3.14, respectively.

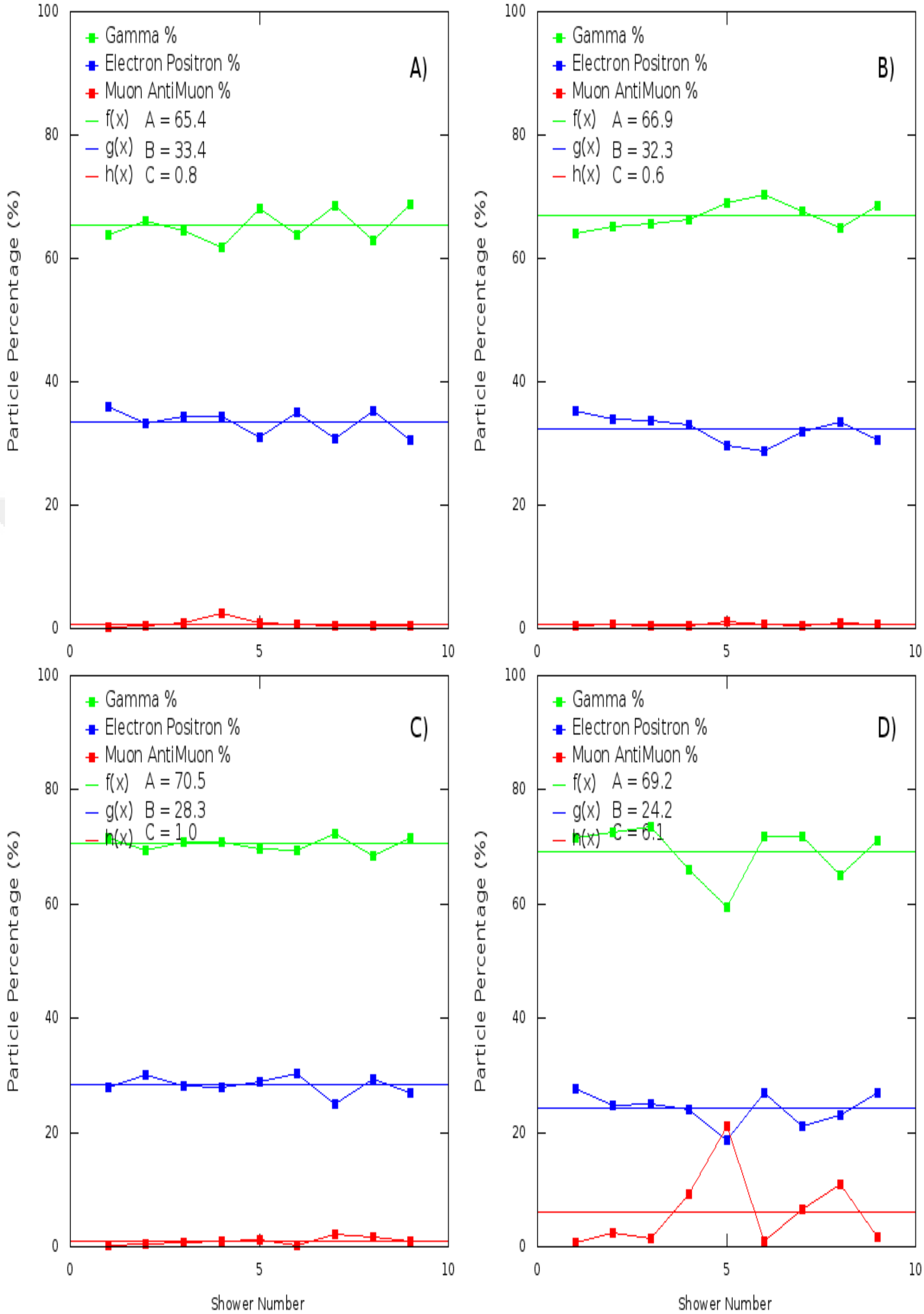

Figure 3.11. According to decay length, particle percentages are shown for gamma (green line), electron-positron (blue line) and muon-antimuon (red line) particles. Particle percentages are fitted a funtions that are f(x), g(x) and h(x) and these fit values are shown on graphs. In this graph, shower energy is $5x10^7$ GeV and distribution of percentages by decay lengths, 3 km, 5km, 7 km and 10 km are shown respectively A,B, C and D.

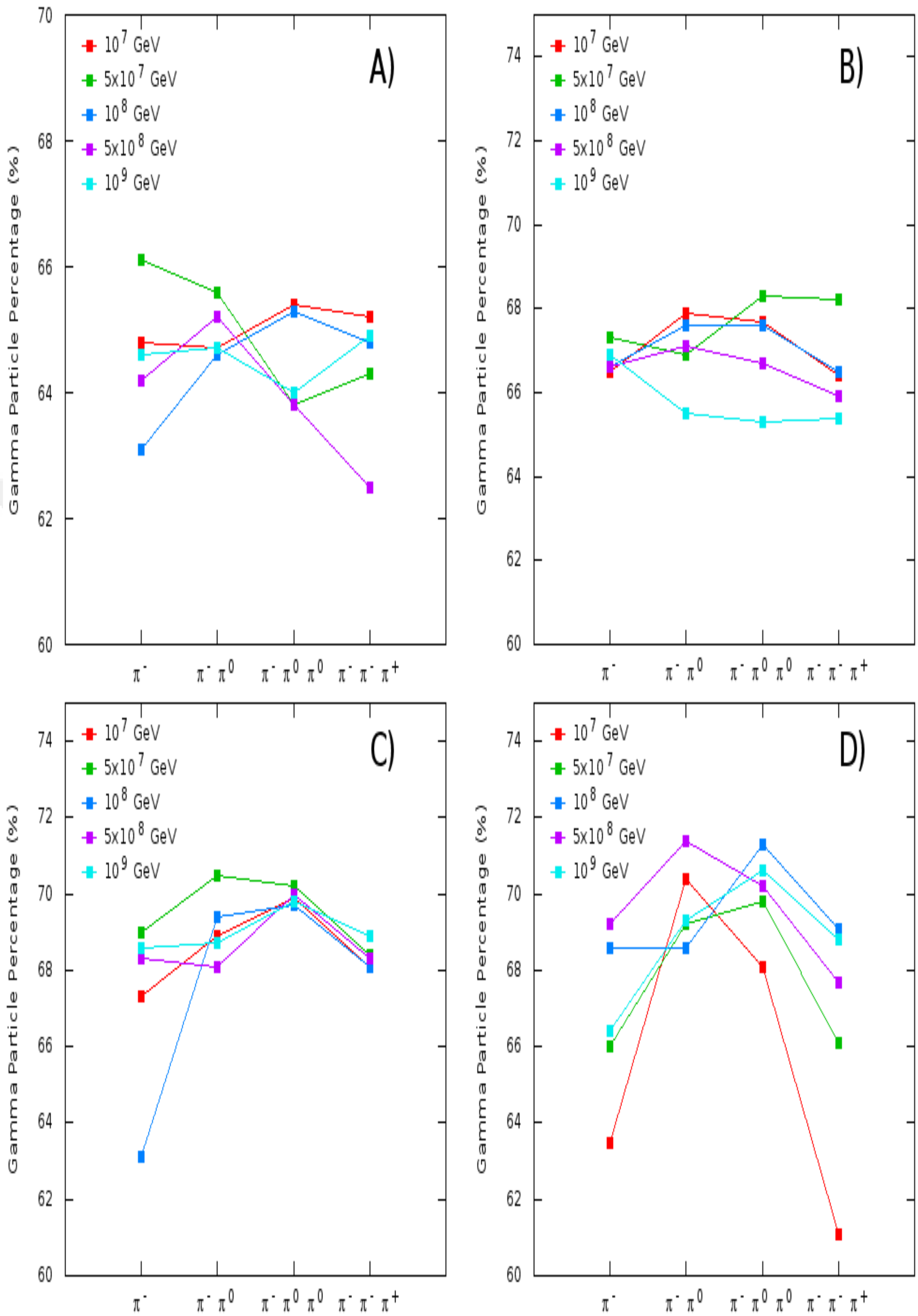

Figure 3.12. Percentages of gamma particles are shown with shower energies in this figure. In the figure, 3 km, 5 km, 7 km and 10 km are shown in A, B, C and D respectively. In the x line of graphs represent decay modes and y line represent percentages of gamma particles on inclined plane.

z

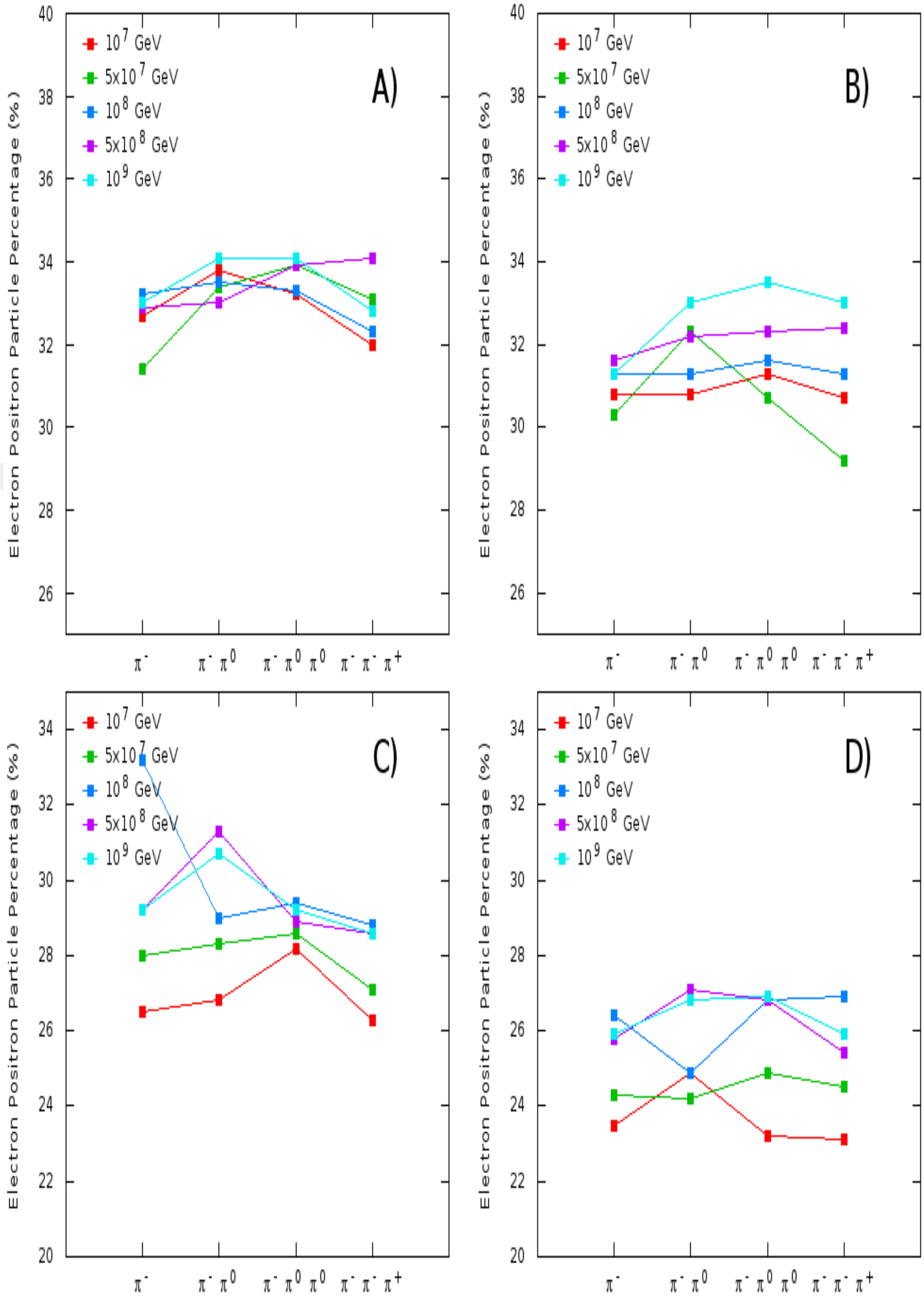

Figure 3.13. Percentages of electron-positron particles are shown with shower energies in this figure. In the figure 3 km, 5 km, 7 km and 10 km are shown in A, B, C and D, respectively. In the x line of graphs represent decay modes and y line represent percentages of electron-positron particles on inclined plane.

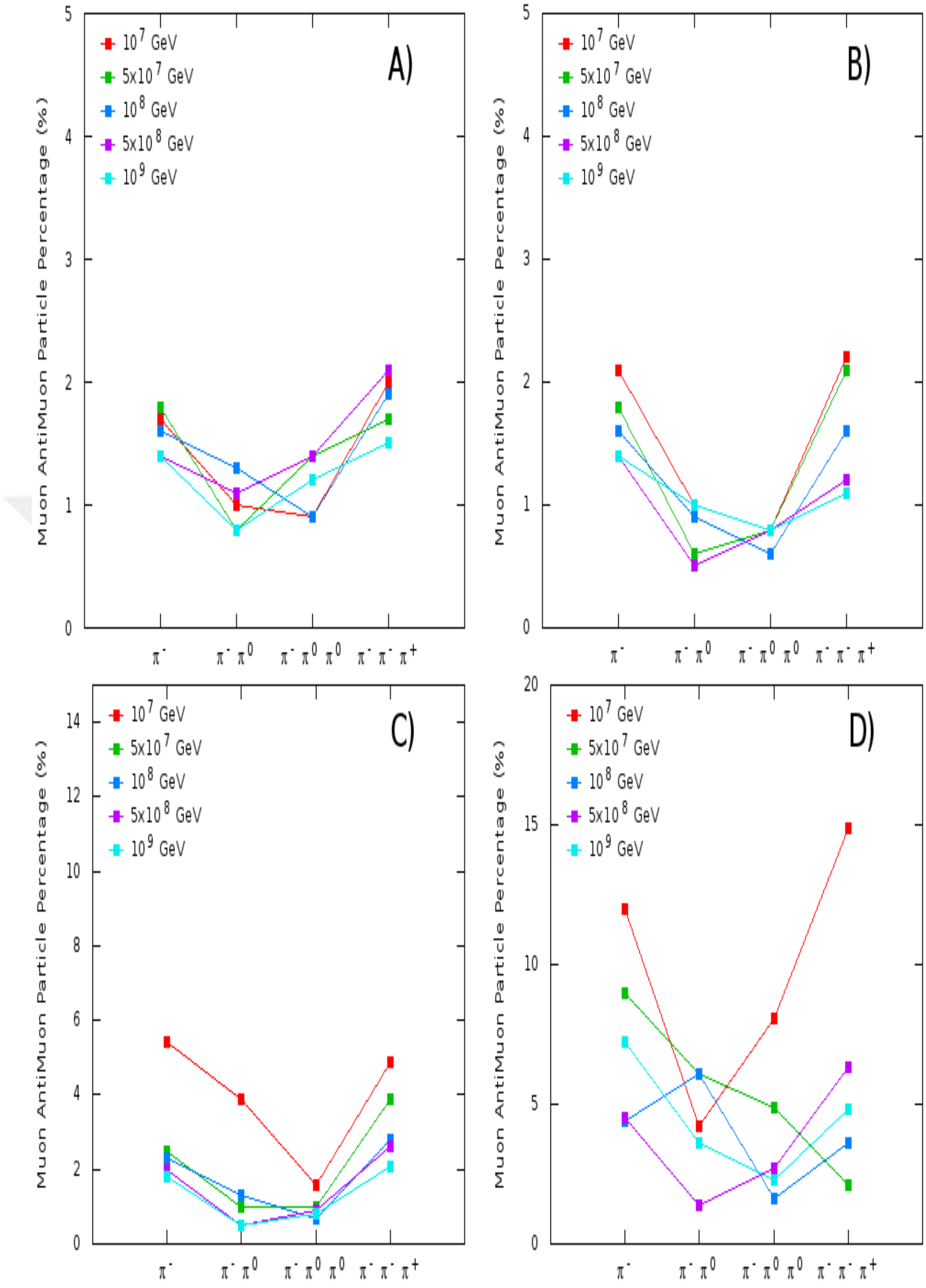

Figure 3.14. Percentages of muon-antimuon particles are shown with shower energies in this figure. In the figure 3 km, 5 km, 7 km and 10 km are shown in A, B, C and D, respectively. In the x line of graphs represent decay modes and y line represent percentages of mu on-antimuon particles on inclined plane.

As mentioned in before, produced electron, positron, muon and antimuon particles decay into gamma particles. If decay length increases, these particles, escipecially electron and postiron particles, decay into gamma particles. As a result of this, percenteges of gamma particles on inclined plane increase as shown in Figure 3.12. In Figure 3.13, the effect of these decays of particles (decay of pions into other particles) are also seen clearly. Percentages of electron and positron particles on inclined plane decreases with incresement of decay length. Moreover, π^0 contribute electromagnetic development of shower and this contribution not only seen in Figure 3.12 but also seen in Figure 3.13. Electromagnetic particle percentages of π^0 related decay modes which are $\pi^- \pi^0$ and $\pi^- \pi^0 \pi^0$ differ from two other decay modes. Even though this diffences can not be seen clearly, percentages of muon and antimuon particles can help to find differences. Also, if this analysis can be made with more than nine showers such as a hundered showers, the difference may be seen clearly without looking percentages of muon and antimuon particles.

As mentioned previously, muon and antimuon particles can travel long distances without decaying. Thus, their percentages is high in longer decay lengths as seen in Figure 3.14. Also, π^- and π^+ contribute abundance of these particles when they are compared with π^0. As a result of these, percentages of these particles are more for π^- and $\pi^- \pi^- \pi^+$ as seen in Figure 3.14.

In short, particle numbers and percentages of inclined plane help to determine shower energy, decay mode and decay length. If these particles can be detected by detectors, estimation of shower energy, decay mode and decay length can be made by using these percentages. However, it need to use more showers for certain results.

3.4 Detector Construction on Inclined Plane

There are many kind of detectors to detect particles and all of them use different methods. This work is based on scintillation detection method by using plastic scintillators and photomultiplier tubes (PMTs). In this method, PMT is linked a plastic scintillator directly and linked system is placed on a box which is closed system for light. When any charged particle goes through box, plastic scintillator produces lights and they are detected by PMT. PMT converts light into signal that read out by computer system. In a nut shell, particle is detected by system.

In this work, scintillation detection method was used to detect particles which produced from tau neutrino shower by simulating a *tower*. Tower is a detector which consist of two boxes with 160 cm separation. Each box contains a two dimensional logical planes with size 20x40 cm^2 as a scintillator and it is refered *tile* in this simulation. As mentioned before, CORSIKA simulation just gives information of shower products on plane. Since simulated tower can recognize particle types with time information and how much particle passes through, PMT was not identified inside of boxes.

In the placement of array, 40 towers on y-axis and 16 towers on z-axis, totally 640 (16, 40) towers were placed on 30 degree inclined plane. Even though distance betwen tower was setted 30 meters along y-axis and z-axis on inclined plane, distance between towers was 15 meters along z-axis because inclination of plane is 30 degree. According to incoming angle of tau neutrino shower, towers were rotated nearly nearly 2.5 degree from horizontal axis. As a result of placement, rectangular shape array of towers was identified in simulation to detect all showers with different energy, decay mode and decay length. Array was needed a center since produced showers were different from each other and they had different distribution on inclined plane in every aspect. Thus, center of array was determined by pre-analysis which gives center of shower products that were on the inclined plane for each shower. Pre-analysis was run for not all particles on the inclined place but also it was run for specific particle like gamma or particle pairs such as electron-positron or muon antimuon pair. Due to scarcity and floating distribution of muon-antimuon particles in showers (Figure 3.15 d,e,f), electron-positron position distribution was used as center of array by determining mean values of x,y and z positions for all electron-positron particles on inclined plane as shown in Figure 3.15 a,b,c. Also, distribution of gamma particles were not take into account, because gamma particles are not charged.

In brief, array of mathematically identified towers were placed in a layout. With the help of placement, detection of showers were aimed with recpect to decay mode, energy and decay length by detecting shower products on inclined plane.

Therefore, 16 tower on z-axis and 40 towers on y-axis were used by 30 meters separation. Moreover, center of array were not determined arbitrarily in order to the density calculation of tower can be done easily.

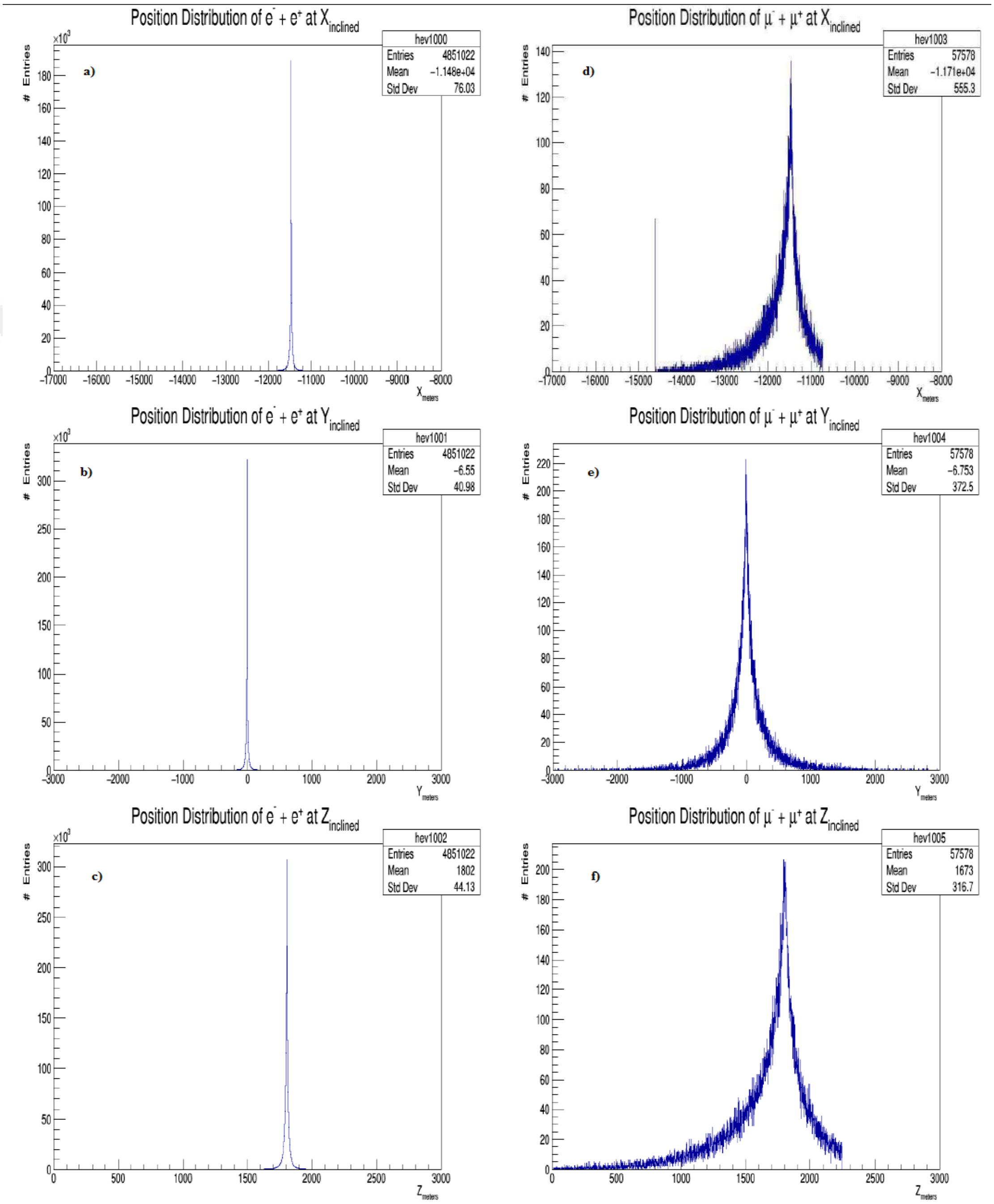

Figure 3.15. Electron-positron particles position distribution x,y and z are shown respectively histogram a,b and c by pre-analysing run10721. Muon-antimuon position distribution x,y and z are shown respectively histogram d,e and f by pre-analysing run10721.

3.5 Particle Detection Strategy

CORSIKA output file includes not only position (x,y,z) information but also momentum (P_x, P_y, P_z, P_{tot}) information of particle on inclined plane for each shower. Using these informations, particles can be counted by towers or tiles. Momentum components of the particles is guide to find direction of particles. If the particle direction is known, detection information of particle can be figured out. Thus, momentum information of particles is used and theta and phi angles is determined with equations.

$$\theta = \arctan\left(\frac{P_x}{P_z}\right) \quad (4.1)$$

$$\varphi = \arctan\left(\frac{P_z}{P_{tot}}\right) \quad (4.2)$$

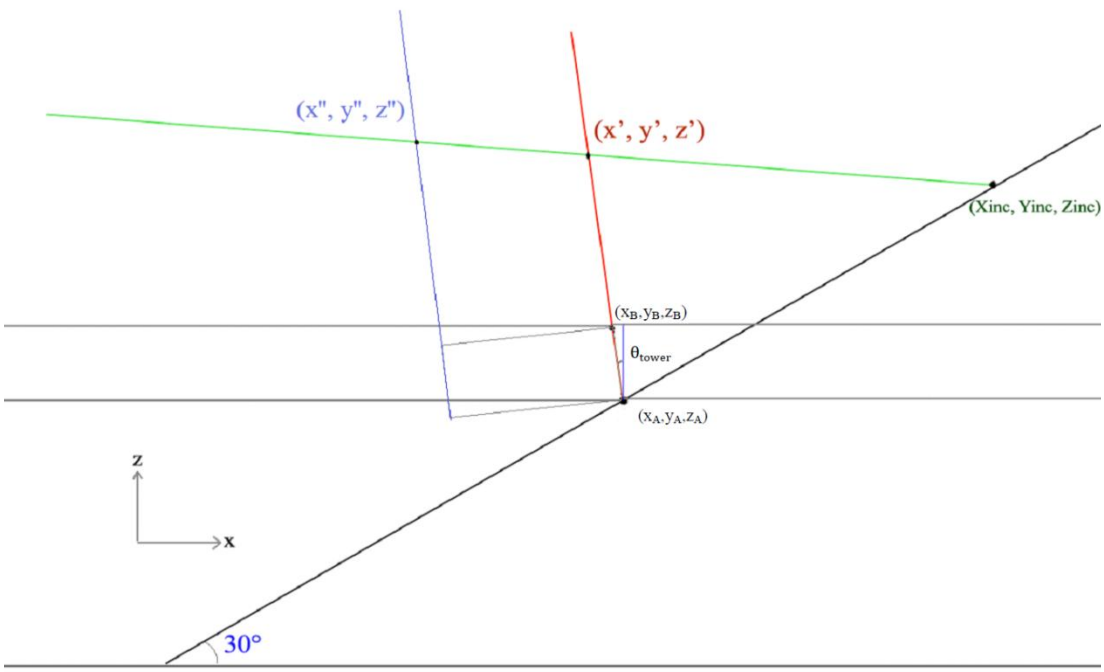

Figure 3.16. Scheme of particle detection strategy is shown by using Z versus Y frame. In this scheme, position of particle is represented as (x_{inc},y_{inc},z_{inc}), first tile is represented as (x_a,y_ac,z_a) and angle of tower is represented as θ_{tower}.

In the particle detection strategy, line intersection points were used to detect particles on inclined plane as shown in Figure 3.16. First of all, using position (x_{inc},y_{inc},z_{inc}), theta (θ) and phi (φ) information of particle on inclined plane, incoming direction line is drawn from a point (x',y',z') as can be written as follows;

$$(x_{inc} - x').\tan\theta = (z_{inc} - z') \quad (4.3)$$

$$(x_{inc} - x').\tan\varphi = (y_{inc} - y') \quad (4.4)$$

Then, a line that passes over tile to a point (x',y',z') is drawn by using positions (x_A,y_A,z_A) and angle of tower θ_{tower} is given by;

$$x' - x_A = \tan(\theta_{tower}).(z' - z_A) \quad (4.5)$$

These lines intersect with each other in a position and that gives intersection point (x',y',z'). Using equations 4.3 and 4.5, intersection point component z' is found as

$$z' = \frac{-z_{inc} + (x_{inc} - x_A + z_A .\tan(\theta_{tower}).\tan(\theta))}{(\tan(\theta_{tower}).\tan(\theta)-1)} \quad (4.6)$$

When z' put into equation 4.3, x' component of intersection point is found as shown;

$$x' = x_A + \frac{\tan(\theta_{tower})}{\tan(\theta_{tower})\tan(\theta)-1}.\left(z_A - z_{inc} + \tan(\theta).(x_{inc} - x_A)\right) \quad (4.7)$$

Then, y' component of intesection point can be found by implanting equation 4.7 to equation 4.4;

$$y' = y_{inc} - \tan(\varphi) \,.\, (x_{inc} - x') \quad (4.8)$$

If intersection points (x',y',z') inside of tile (x_A,y_A,z_A) and (x_B,y_B,z_B) which close to inclined plane, particle is detected by first tile. Although second tile x and z position need to be different, equations of intersection points is same. Thus, second tile intersection points (x",y",z") can be found. If particle is detected by first tile and second tile, it is detected by tower. Detected electron and positron particles by first tile are shown in Figure 3.17 with different view. Similarly, detected electron and positron particles by second tile are shown in Figure 3.18 and by tower is represented in Figure 3.19.

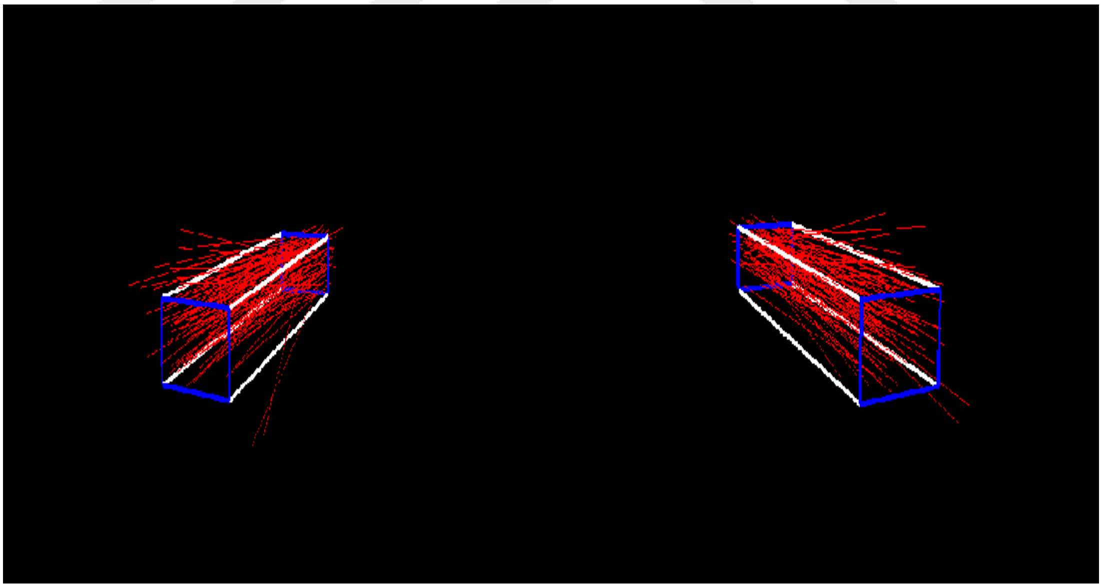

Figure 3.17. Using intersection points detected electron and positron particles by first tile are shown with different tower view (left and right side) in figure. Tower is member (7,19) of tower array (16,40) and run10721 were used for figure.

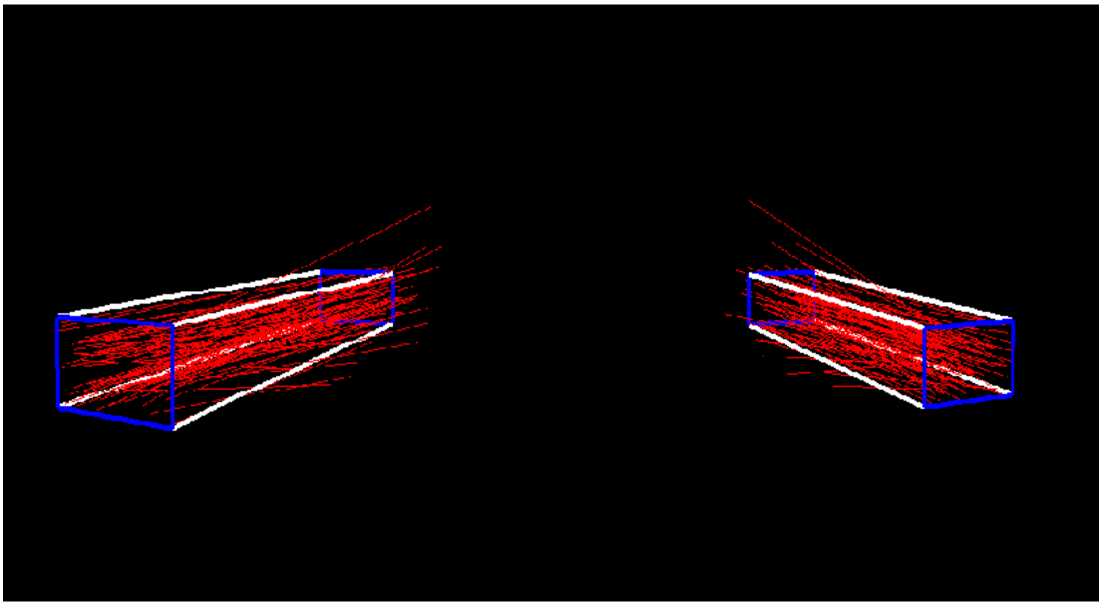

Figure 3.18. Using intersection points detected electron and positron particles by first second tile are shown with different tower view (left and right side) in figure. Tower is member (7,19) of tower array (16,40) and run10721 were used for figure.

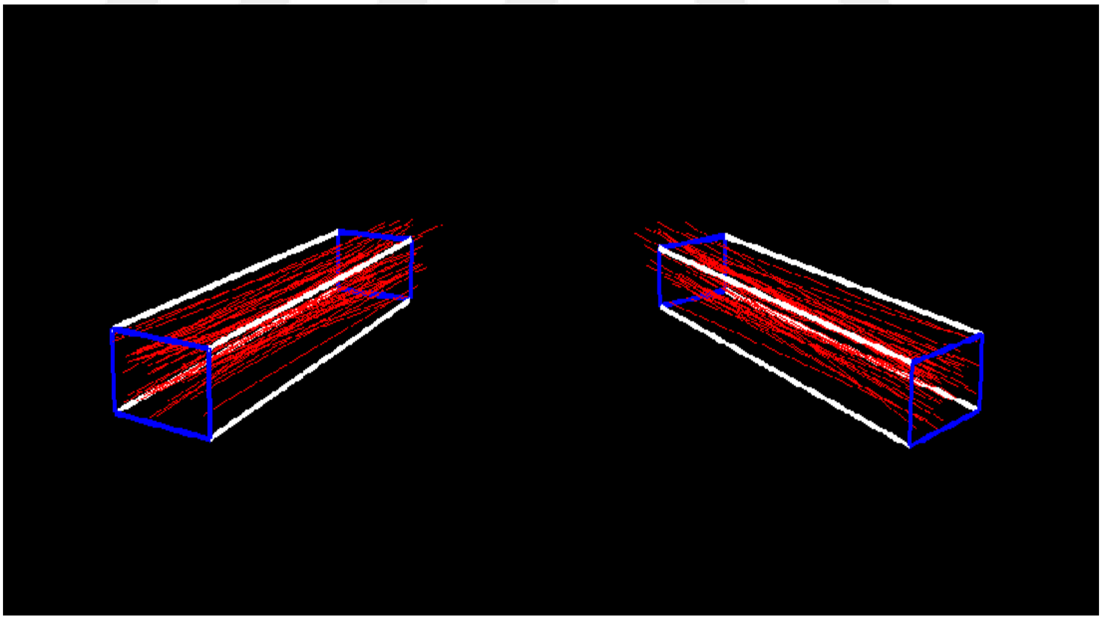

Figure 3.19. Using intersection points detected electron and positron particles by first tower are shown with different tower view (left and right side) in figure. Tower is member (7,19) of tower array (16,40) and run10721 were used for figure.

In conclusion, particles on inclined plane can be detected by towers of array and also particle densities can be calculated for each tower, or tiles. Moreover, with this strategy particles dentsities of tower or tile can be recognized for particle pair such as electron-positron (electromagnetic component of shower) or muon-antimuon (hadronic component of shower). In the following sections, showers with different energy, decay modes and decay length will analyzed with this strategy and result will be represented.

3.6 Analysis Code of Simulation

Analysis code of simulation is based on detectors construction on inclined plane and particles detection strategy of tower sections of this chapter. It is written in C++ programming language with using ROOT dependencies and classes (ROOT Web Page). In this section, analysis code of simulation will be expressed shortly.

Analysis code of simulation consists of two parts. First part of the code places logical towers in certain manner by using center information of particles on inclined plane. As mentioned previously, center of array can be different shower by shower because of total number of electron-positron particles on plane. Thus, center of array information is obtained by pre-analysis before main analysis. Then, obtained center of array is used by the first part of code to place towers for each shower without exception. In this placement, specified layout is applied on inclined plane and code keeps informations of tower locations.

In the second part of the code, particle detection strategy is performed by using tower locations and momentum informations of particles. As mentioned previously, particle detecting strategy depends on intersection points. This dependency is written in the second part of code, since tower locations need to be defined in code. In the algorithm, theta and phi angles are calculated for a particle on inclined plane. Then, intersection points are calculated for each tower and its tiles by using these angles. If intersection point is inside of any tile or tower, particle detection information is counted. This algorithm makes same calculations for all particles on inclined plane. Although simulation based on scintillation method, logically defined towers can detect all kind of particles such as electron, muon, gamma etc. with the help of the analysis code. At the end, second part of the code writes total counts of detecting particles on the array tower by tower and tile by tile to use other analysis.

3.7 Analysis of Tower Array

In this section, sum of detected partciles on the array will be represented with graphs. For this work, $\pi^- \pi^0$ showers that were produced with $5x10^7$ GeV shower energy and 3, 5, 7 and 10 kilometers decay lengths will be detailed according to sum of detected particles.

Sum of total detected particles on the array is not only important to determine differences between other showers is produced with different decay modes, shower energies and decay lengths, but also it shows differences between decay lengths of showers which produced with same shower energy and decay mode. Moreover, detected electromagnetic and hadronic components of showers can give clue about decay mode of shower. However, results of whole analysis will be discussed in the results and discussion chapter by using produced graphs of this section.

Even though nine showers is produced with same shower energy and decay mode, distribution of detected particles on towers and tiles can be different. Therefore, distribution of detected particles by first tile are fitted a function, f(x) = m,which gives mean values of nine showers. Also, this analysis is made for all detected particles and specific particles or particle pairs such as gamma particles, electron-positron particles and muon-antimuon particles. As seen in Figure 3.20, 3.21, 3.22 and 3.23, sum of all detected particles of nine showers with different decay lengths are shown with mean values. Similarly, sum of detected gamma, electron-positron and muon-antimuon particles of nine showers with different decay lengths is shown with mean values in these figures. Meanwhile, other showers which were produced with different decay modes, shower energies and decay lengths will be represented Appendix B with mean value tables. In all graphs, red line represents sum of particles which are detected by first tiles of towers and blue line represents sum of particles which are detected by second tile of towers. Similarly, green line represents sum of detected particles by towers. Black line is represents mean value of detected particles by using first tile values.

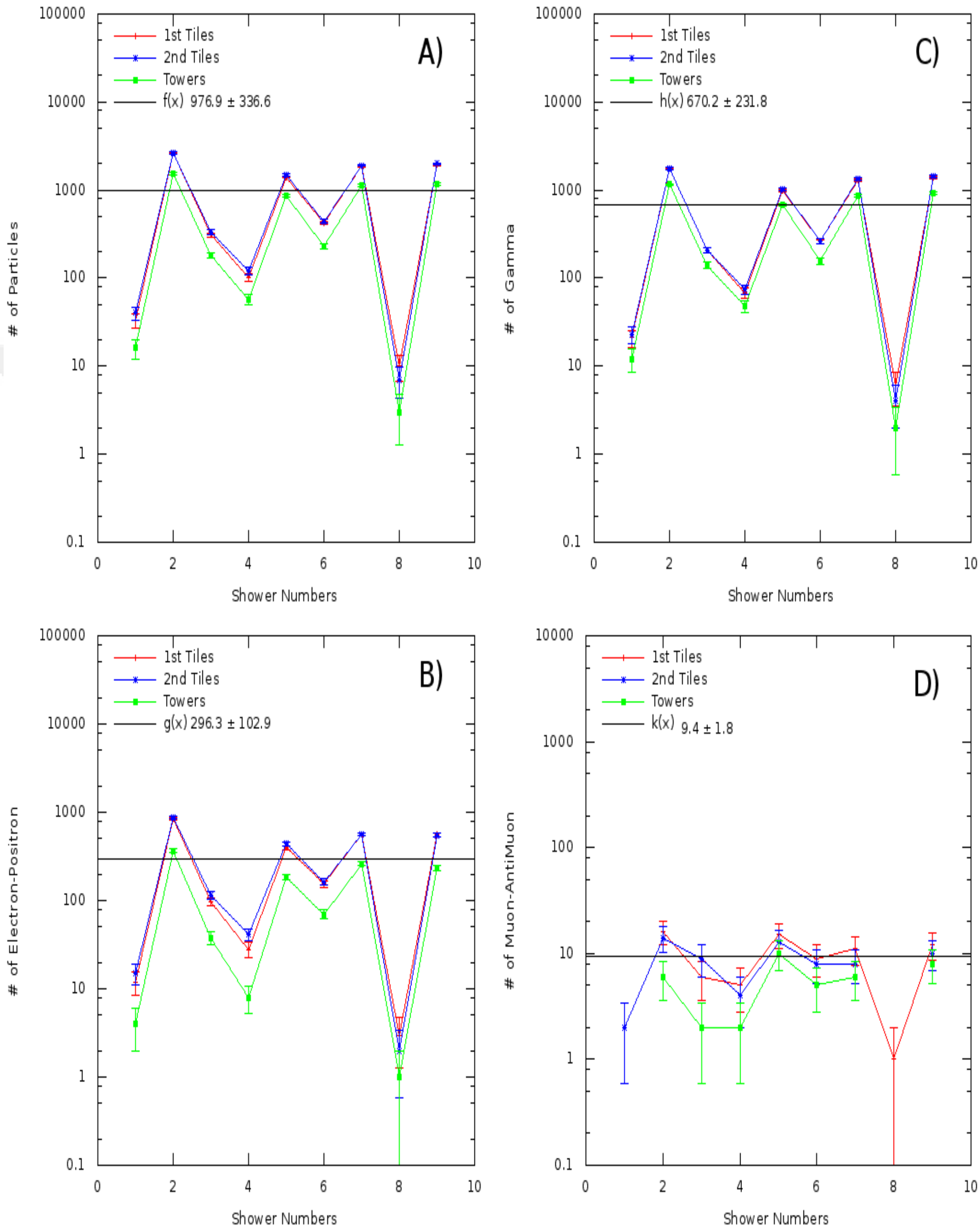

Figure 3.20. Sum of all detected, electron-positron, gamma, muon-antimuon particles by towers and tiles are shown shower by shower with using same shower energy ($5x10^7$ GeV) and decay length which is 3 km with respect to A, B, C and D for $\pi^- \pi^0$ showers. As seen in figure, mean values of detected particles of nine showers are determined by fitting first tile values of showers to f(x) = m function for all decay lengths.

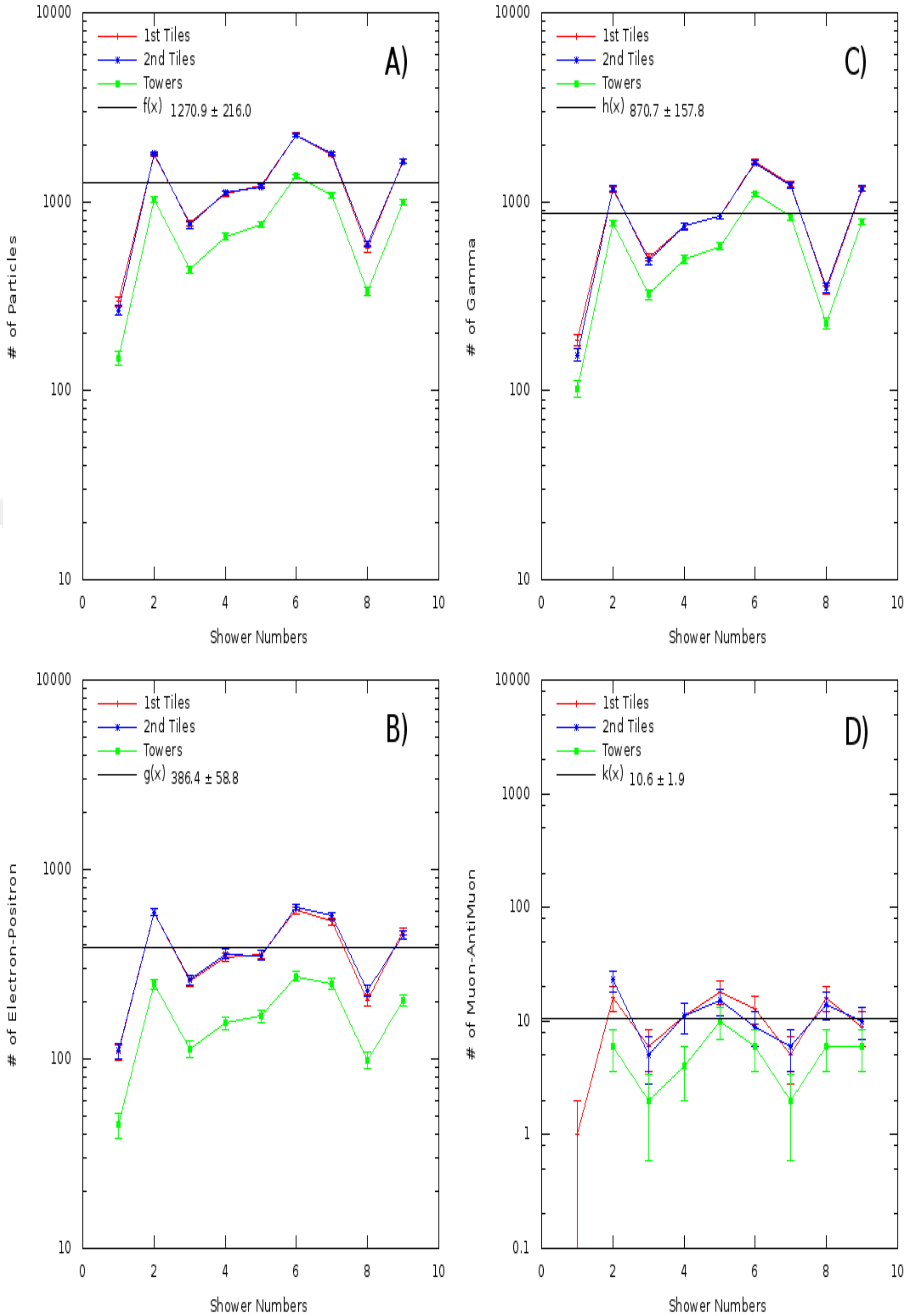

Figure 3.21. Sum of all detected, electron-positron, gamma, muon-antimuon particles by towers and tiles are shown shower by shower with using same shower energy ($5x10^7$ GeV) and decay length which is 5 km with respect to A, B, C and D for $\pi^- \pi^0$ showers. As seen in figure, mean values of detected particles of nine showers are determined by fitting first tile values of showers to f(x) = m function for all decay lengths.

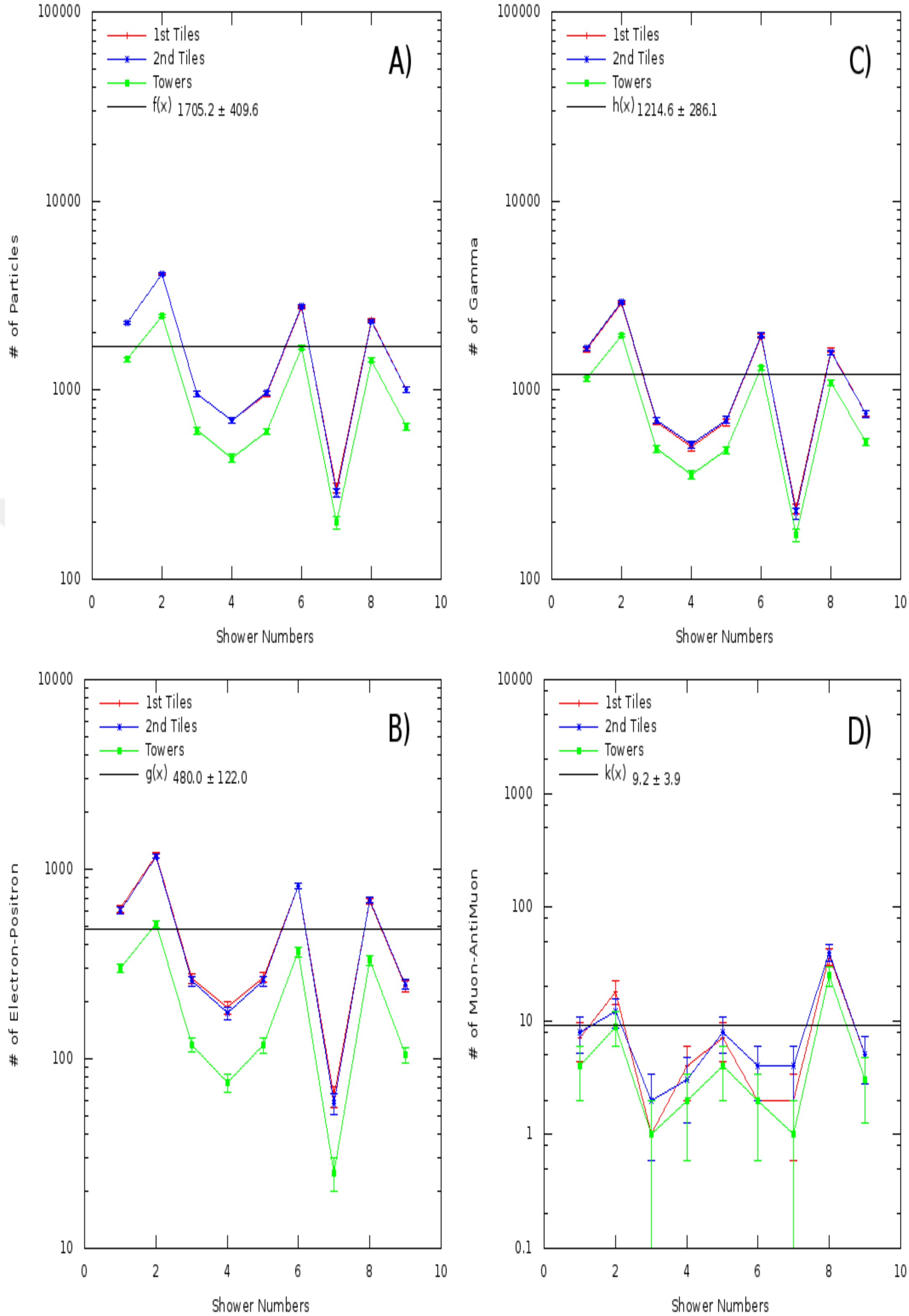

Figure 3.22. Sum of all detected, electron-positron, gamma, muon-antimuon particles by towers and tiles are shown shower by shower with using same shower energy (5x10^7 GeV) and decay length which is 7 km with respect to A, B, C and D for $\pi^- \pi^0$ showers. As seen in figure, mean values of detected particles of nine showers are determined by fitting first tile values of showers to f(x) = m function for all decay lengths.

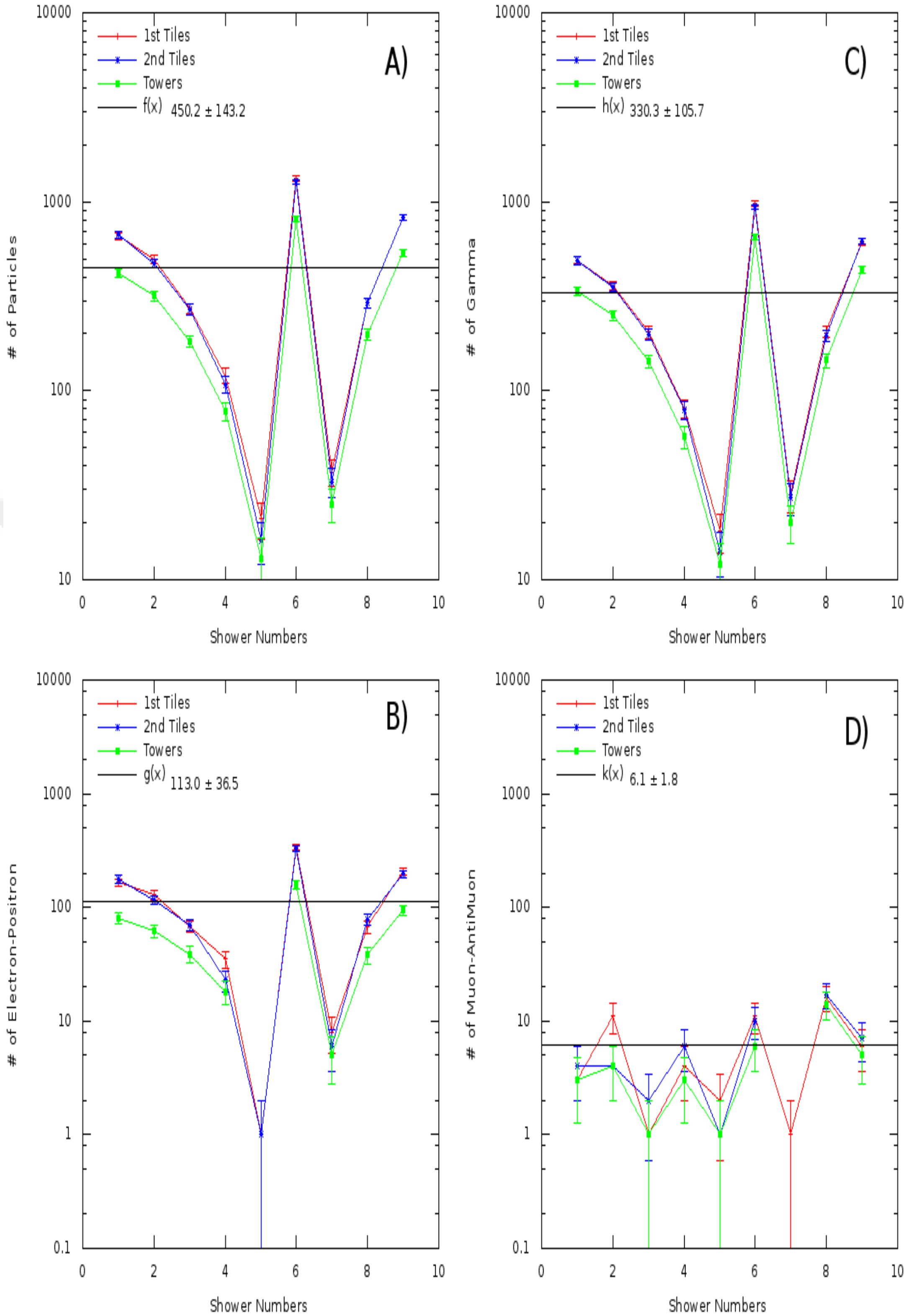

Figure 3.23. Sum of all detected, electron-positron, gamma, muon-antimuon particles by towers and tiles are shown shower by shower with using same shower energy ($5x10^7$ GeV) and decay length which is 10 km with respect to A, B, C and D for $\pi^- \pi^0$ showers. As seen in figure, mean values of detected particles of nine showers are determined by fitting first tile values of showers to f(x) = m function for all decay lengths.

3.8 Analysis of Central Towers with Particle Densities

In this section, particle densities of central towers and their tiles will be represented with electromagnetic components and hadronic components. For this work, $\pi^- \pi^0$ showers that were produced with $5x10^7$ GeV shower energy and 3, 5, 7 and 10 kilometers decay lengths will be detailed.

According to positions of towers, number of detected particles by towers and their tiles fluctuate when tower array is considered tower by tower. Particle numbers on inclined plane decreases with moving away from shower core. Since tower array were placed by using position distribution of particles, number of detected particles by central towers and their tiles are much more than other towers on the array. Thus, 16 towers were selected on center of array to determine profile of showers by taking into consideration decay mode, shower energies and decay lengths. In Figure 3.24, selected towers from whole array is shown inside of red square. In the figure, center of array can be seen at the rigth side of graph. Moreover, detected particle numbers on selected towers were used to determine particle densities of their locations in this study. Due to location of first tiles on towers which are close to inclined plane, first tiles were used to calculate densities of tiles. Also, densities of towers were calculated approximately by dividing number of detected particles on tile to tile area and shown all of graphs. In the graphs, first tile which was highly fired by particles was selected central from towers to find mean density values of nine showers by fitting function like f(x) = m and the line of function is shown. All densities and sum of detected particles were shown with representing first tiles of the showers.

In this study, all showers with produced different decay mode, energy and decay length were deeply investigated and tables of mean values will be detailed in Appendix B. Densities of selected towers examined in two groups which are detected charged electromagnetic particles and hadronic particles. This section will follow these two groups by graphs in the subsection of this section. However, results of this study will be discussed results and discussion chapter with comparising decay modes, energies and decay lengths.

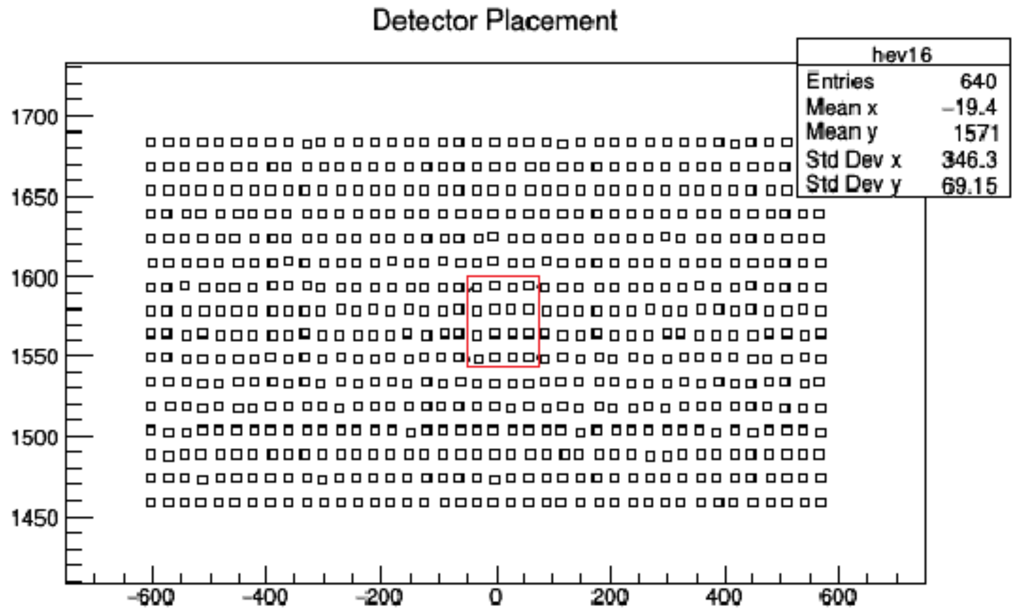

Figure 3.24. First tiles of towers are shown representatively by using run10721 array placement. Selected central tiles are shown inside of red square. Their row and column numbers are [7:19], [7:20], [7:21], [7:22], [8:19], [8:20], [8:21], [8:22], [9:19], [9:20], [9:21], [9:22] , [10:19], [10:20], [10:21], [10:22] with respect to [16:40] array placement. In figure, units of X line and Y line are meters.

3.8.1 Detected Electromagnetic Components by Central Towers

In this subsection, detected electon-positron particle pairs by central tiles of towers will represented for $5x10^7$ GeV, $\pi^- \pi^0$ showers with 4 different decay lengths as mentioned previously.

The aim of this study determine the charged electromagnetic particles and densities on central tiles. With the help of these densities, not only decay modes of showers can be distinguished from each other by using mean values of graphs, but also relation about decay lengths can be lighten. Moreover, densities of tiles can give a clue about behaviour of showers according to their features. Additionaly, abundance of charged electromagnetic particles in the showers can be used to determine the profile of the showers which were produced by using same decay modes, shower energies and decay lengths.

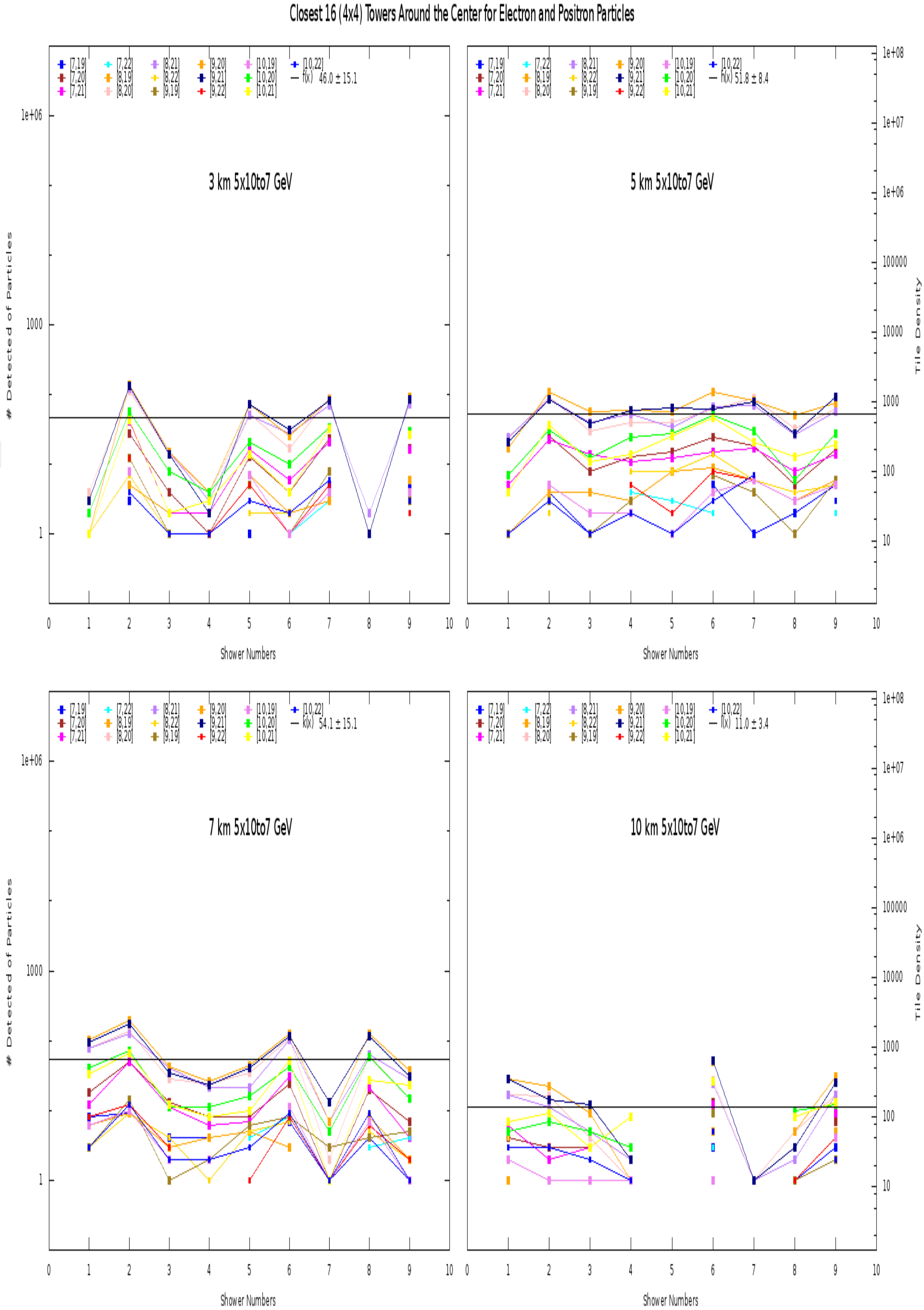

Figure 3.25. This figure represents densities of tiles on central towers. Most fired tiles were fitted a function which gives mean values of densities of showers with respect to electron-positron particles.

As seen in Figure 3.25, mean values of detected electron-positron particles were obtained by fitting funtion. Besides, most fired tiles are generally center of the array and this makes it easy for energy discrimination. Comparison of all these mean values with respect to shower energy, decay mode and decay length will be discussed in results and discussions section of thesis.

3.8.2 Detected Hadronic Components by Central Towers

In this subsection, detected muon-antimuon particle pairs by central tiles of towers will represented for $5x10^7$ GeV $\pi^- \pi^0$ showers with 4 different decay lengths.

According to distribution of these particles, central towers were not fired with these particles. Thus, mean values of these particles cannot be calculated for low energies. However, with more produced tau neutrino induced shower these mean values can be calculated and according to these mean values discrimination can be made. In Figure 3.26, muon-antimuon particle densities are shown by using central towers. As seen in the figure, scarcity of these particles can be seen clearly.

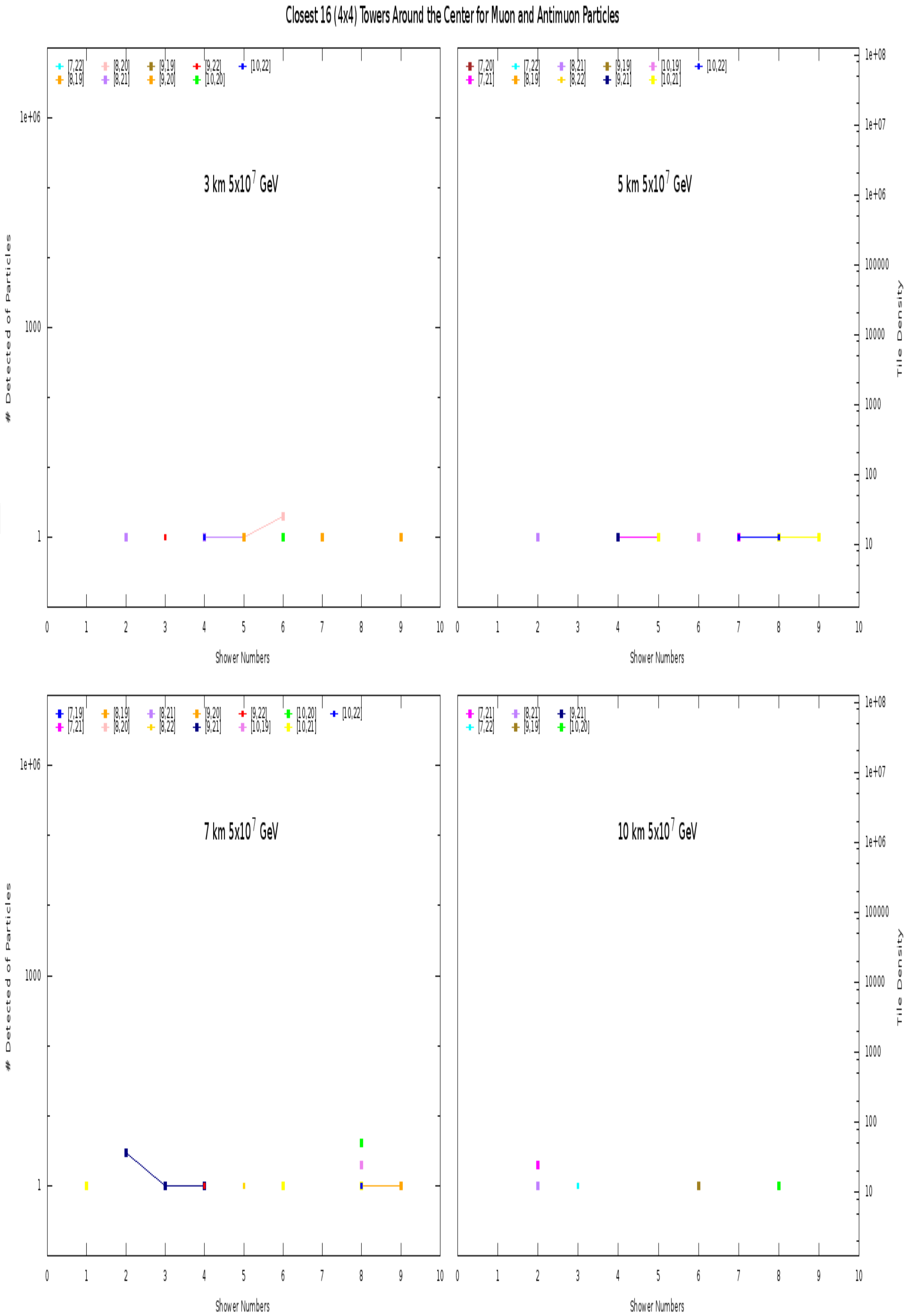

Figure 3.26. This figure represents densities of tiles on central towers. Most fired tiles were fitted a function which gives mean values of densities of showers with respect to muon-antimuon particles.

4. RESULTS AND DISCUSSION

In this chapter, analysis results of detection of tau neutrino induced showers will be discussed by comparing shower energy, decay mode and decay length. With the help of these, profile of tau neutrino induced showers will be explained for earth skimming strategy.

As mentioned in previous chapter, detected particles on tiles were investigated shower by shower and sum of these particles were seperated as electron-positron and muon-antimuon particle pairs. These seperated pairs were plotted and fitted a function that calculated mean values of investigated shower energy, decay mode and decay length. In Appendix B, used graphs are represented by mean values. These mean values are plotted as shown in Figure 4.1. As seen in figure clearly, number of detected electron-positron particles on first tiles of array increase with the incresement of energy. The number of detected electron-positron particles reach maximum at 5 km decay length and minimum at 10 km decay length. However, number of detected electron-positron at 7 km and 5 km are close which indicates that shower reaches the maximum size between these two decay lengths. Distinction of decay modes can be hard to recognize except π^- decay mode because of low detected electron-postiron particles. For decay mode prediction, muon-antimuon particles were used to discriminate decay modes. In Figure 4.2, mean values of detected muon-antimuon particles were plotted. According to figure 4.2, $\pi^- \pi^- \pi^+$ decay mode can be distinguished from other decay modes. However, other decay modes cannot be separeted from each other.

In theory, decay modes which contains π^+ or π^- must have more muon and antimuon particles than π^0 related decay modes. Also, incresement of decay length must increase muon-antimuon numbers and decrease electron-positron numbers. Thus, percentages of these particles pairs were calculated according to their detected particles mean values. These percentages were plotted as seen in Figure 4.3 and 4.4 which show that confirmation of theory seen clearly for every aspect. For example, π^0 related decay modes contributes electron-positron percentages on tiles of array and pencentages of them decrease with increasement of decay length. On the other hand,

π^+ or π^- related decay modes contributes muon-antimuon percentages on tiles of array and pencentages of them increase with increasement of decay length. These graphs are also shown that the larger part of detected particles are electron-postiron particles on tiles.

Densities of central tower tiles were investigated and results energy prediction can be made by these tile densities. Since energy seperation of these tiles seen clearly as seen in Figure 4.5. For these figures, most densed tile were selected from center of array with respect to electron-postiron particles.Then, mean values of showers according to their varibles were calculated to determine energy seperation. However, mean values for muon-antimuon densities of central towers cannot be calculated because of scarcity of these particles. As shown in previous chapter, these particles are scattered around not like electron-positron particles on inclined plane. Also, scarcity of these particles on inclined plane is another negative effect preventing us to use muon-antimuon particles for analysis.

In Figure 4.5, energies of shower can be distinguished from each other except π^- decay mode. Besides, not only development of shower is confirmed again for 5 km decay length but also fading of shower can be recognized for 10 km decay length.

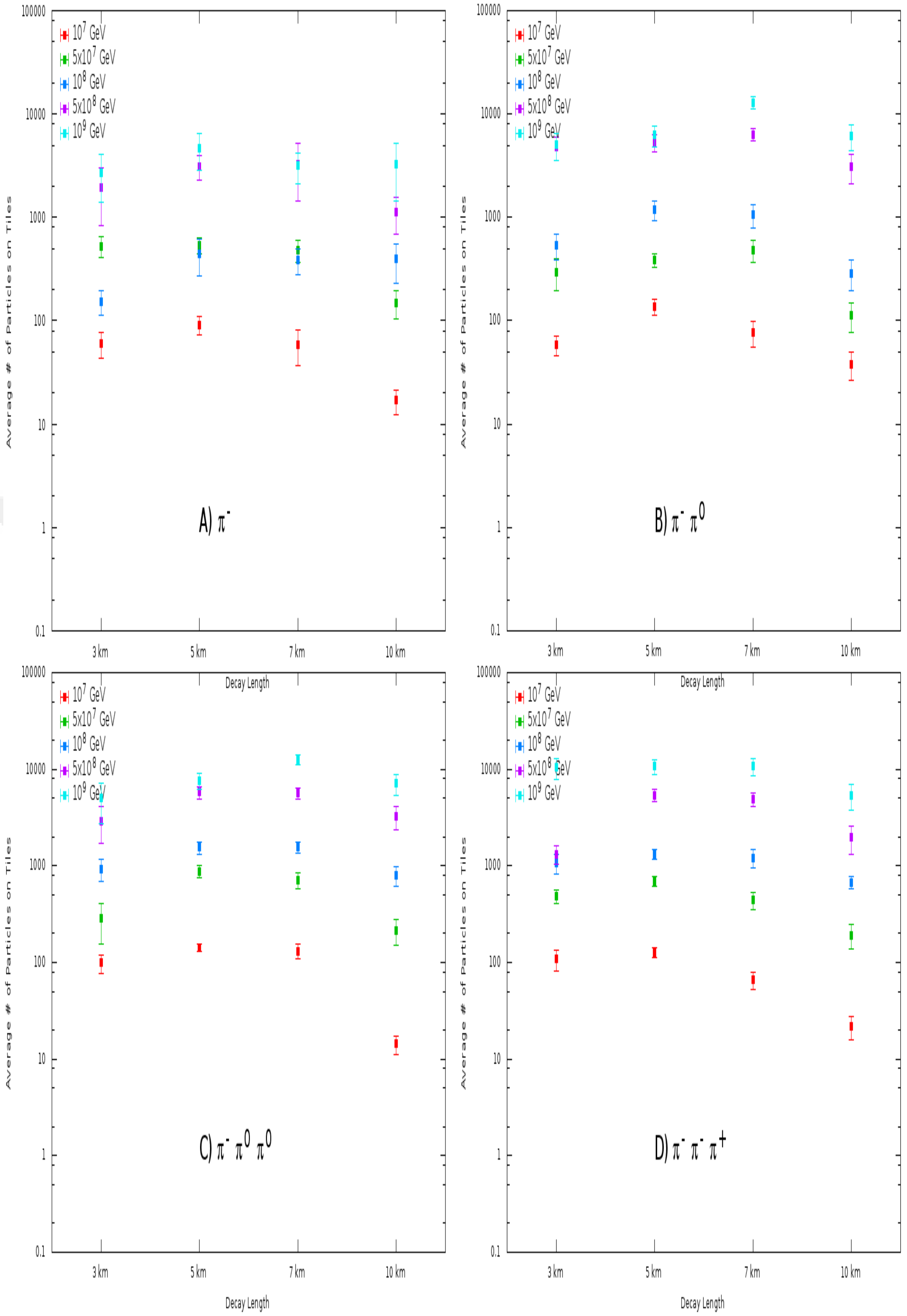

Figure 4.1. Distribution on number detected electron-positron particles by tiles of array which are gained by fitting a function for all energies and decay lengths is represented with regard to decay length. π^-, $\pi^-\ \pi^0$, $\pi^-\ \pi^0\ \pi^0$ and $\pi^-\ \pi^-\ \pi^+$ decay modes are shown respectively in A ,B, C and D parts of figure.

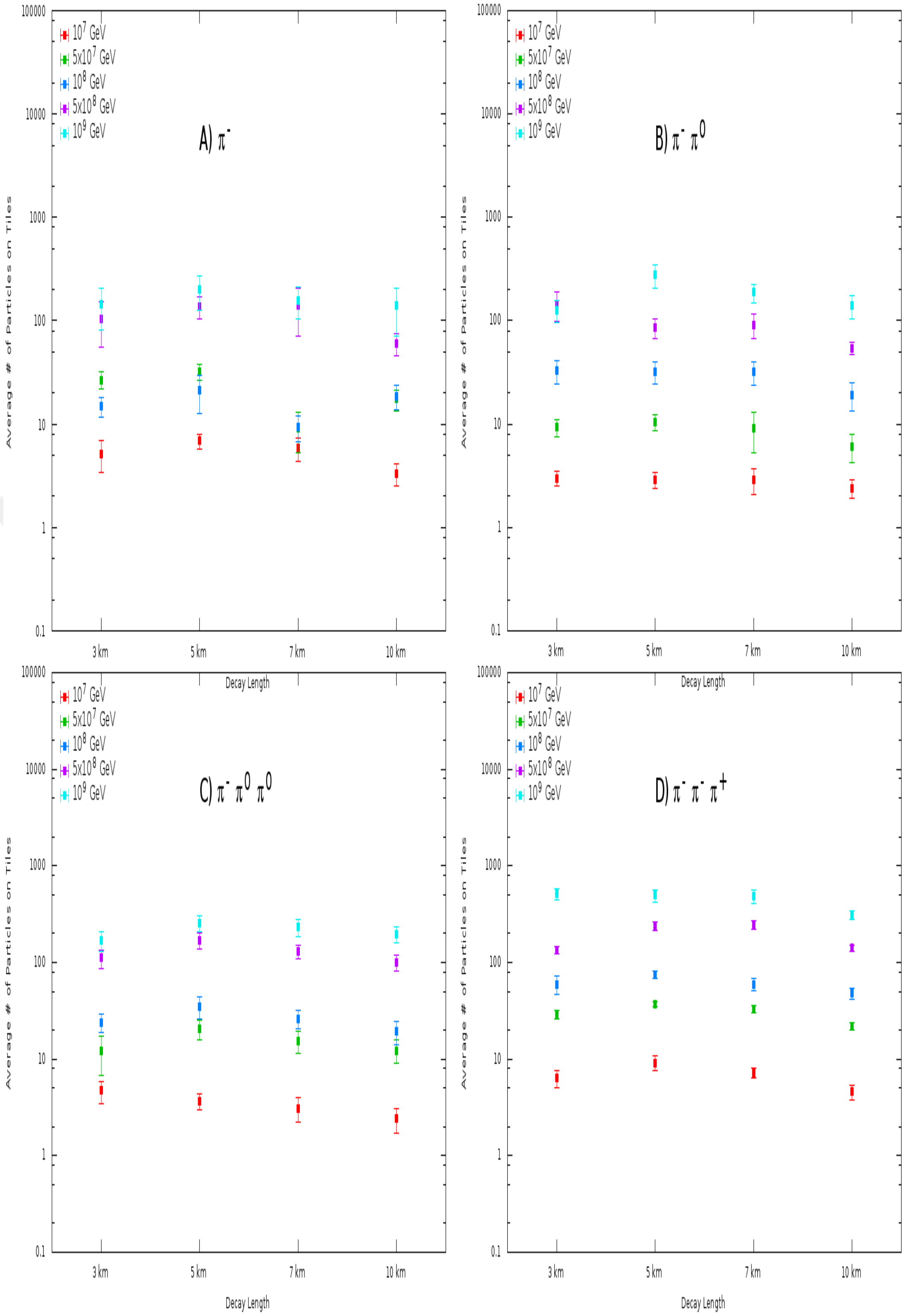

Figure 4.2. Distriution on number detected muon-antimuon particles by tiles of array which are gained by fitting a function for all energies and decay lengths is represented with regard to decay length. π^-, π^- π^0, π^- π^0 π^0 and π^- π^- π^+ decay modes are shown respectively in A, B, C and D parts of figure.

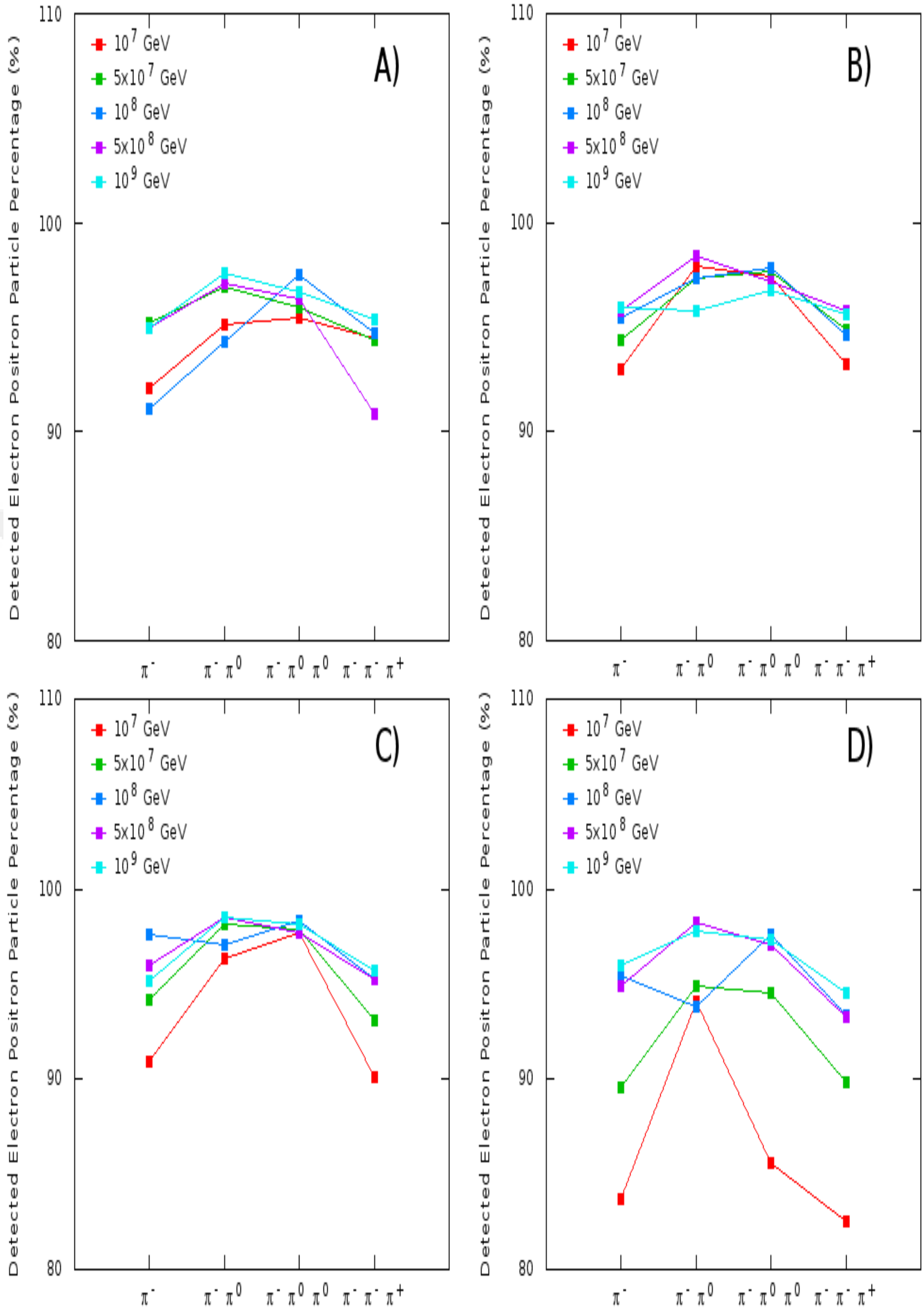

Figure 4.3. Percentages of detected electron-positron particles by tiles of array are shown with shower energies in this figure. In the figure, 3 km, 5 km, 7 km and 10 km are shown in A, B, C and D, respectively. In the x line of graphs represent decay modes and y line represent percentages of electron-positron particles that were caught by first tiles of towers.

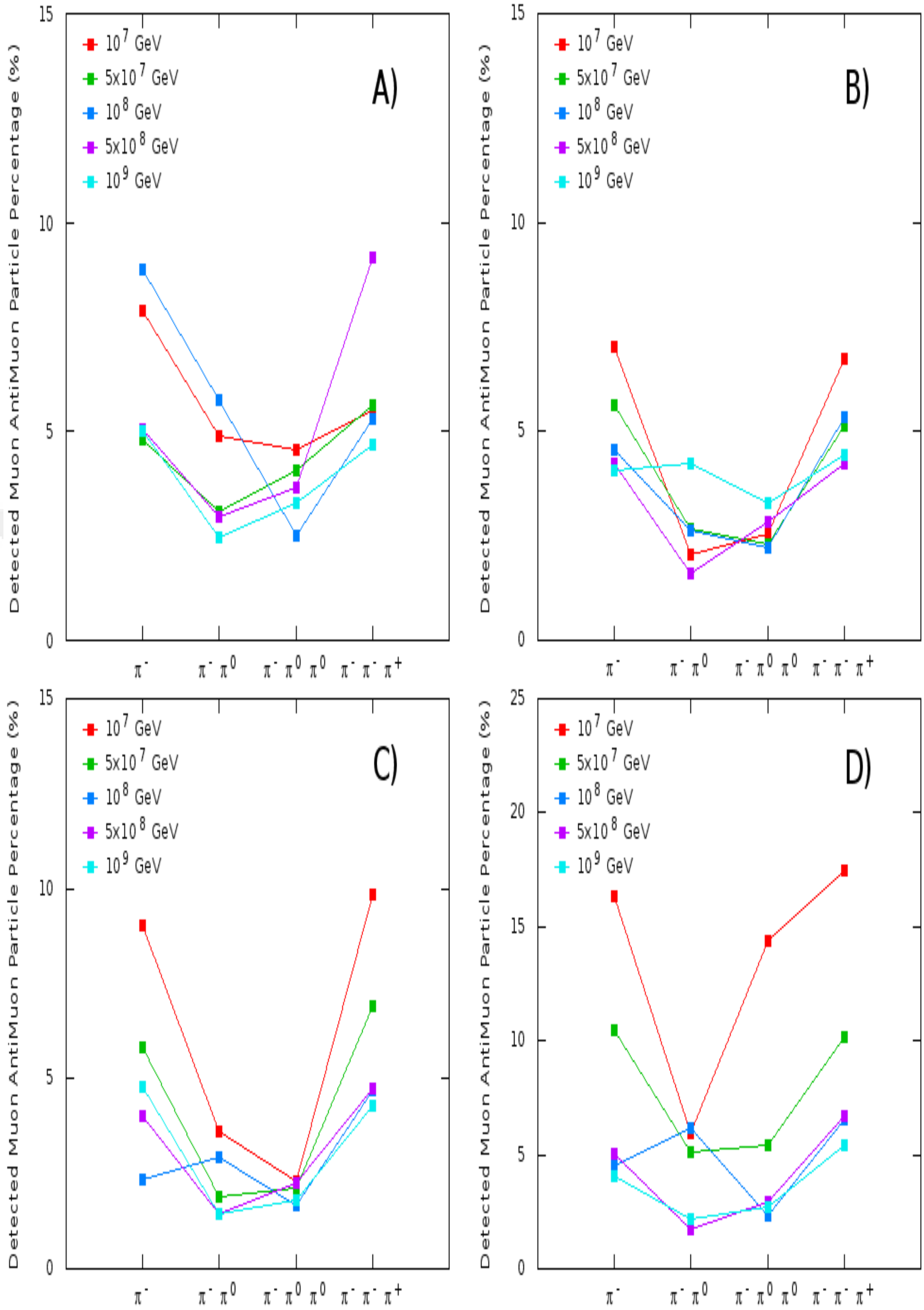

Figure 4.4 Percentages of detected muon-antimuon particles by tiles of array are shown with shower energies in this figure. In the figure 3 km, 5 km, 7 km and 10 km are shown in A, B, C and D, respectively. In the x line of graphs represent decay modes and y line represent percentages of muon-antimuon particles that were caught by first tiles of towers.

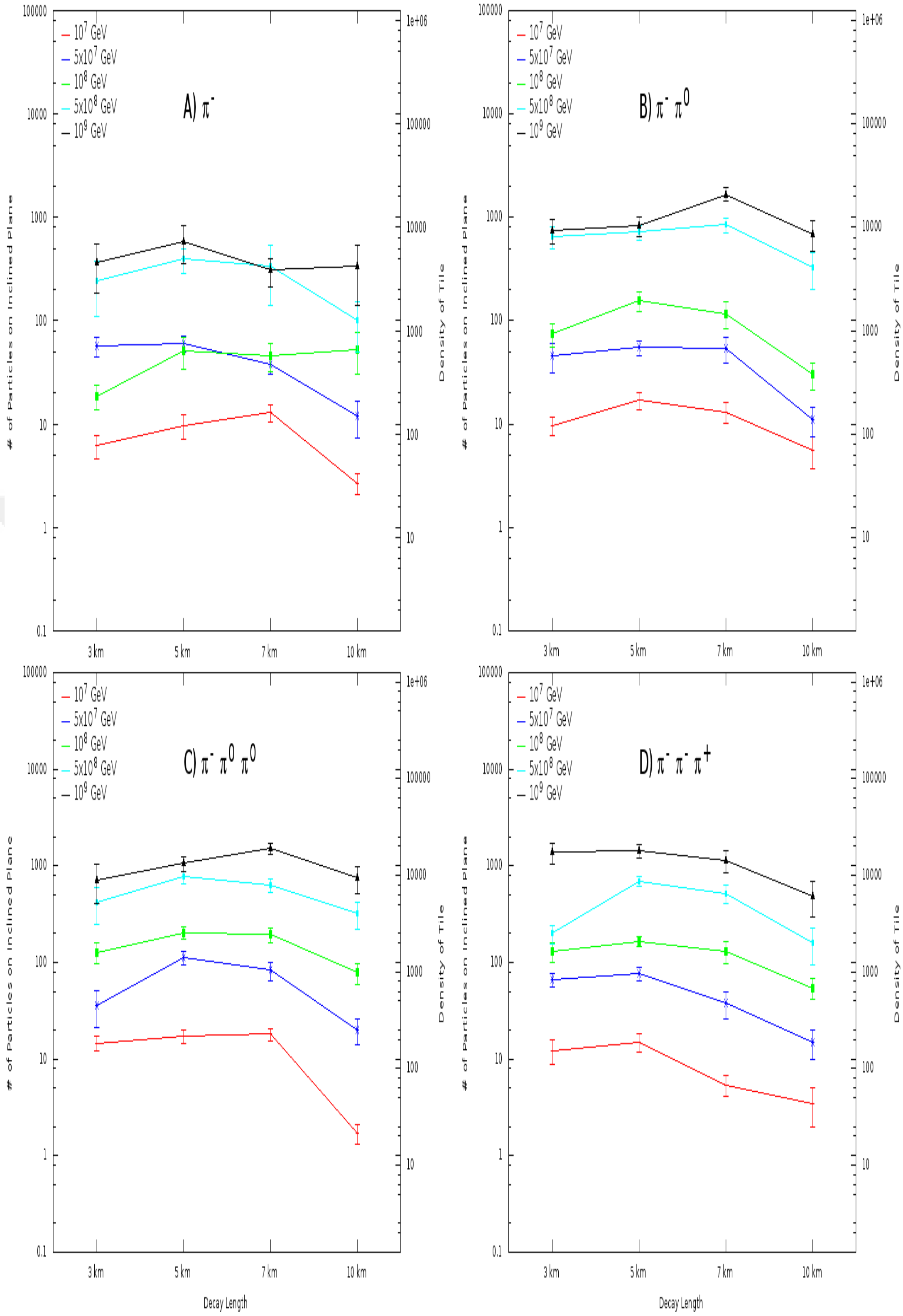

Figure 4.5. Distribution of number detected electron-positron particles by central tiles of array which are gained by fitting a function for all energies and decay lengths is represented with regard to decay length. π^-, $\pi^-\ \pi^0$, $\pi^-\ \pi^0\ \pi^0$ and $\pi^-\ \pi^-\ \pi^+$ decay modes are shown respectively in A, B, C and D parts of figure.

5.CONCLUSIONS AND RECOMMENDATIONS

This work shows that, tau neutrino induced showers can be detected by earth skimming strategy and also they can be seperated from each other with respect to their energy, decay mode and decay length. These results are improtant for neutrino astronomy and cosmic rays spectroscopy. With the help of simulations, these showers can be determined with variables. Moreover, energy spectrum of cosmic rays can be determined experimantally. However, these results can be flourished by simulating and analyzing more tau neutrino induced showers by CORSIKA program.

In conclusion, this work shows that tau neutrino induced shower can be determined and profile of these showers can be obtained with these analysis. For further analysis like angle of these kind showers can be determine using these gained variables and certain results of these showers can be made with using this analysis.

6. REFERENCES

Abbasi R and IceCube Collaboration (2010a) "The IceCube Data Acquisition System: Signal Capture, Digitization, and Timestamping", Nuclear Instruments and Methods A. 601: 294–316.

Abbasi R and IceCube Collaboration (2010b) "Calibration and Characterization of the IceCube Photomultiplier Tube", Nuclear Instruments and Methods A. , 618: 139–152 .

Abreu P and Pierre Auger Collaboration (2013) "Ultrahigh Energy Neutrinos at the Pierre Auger Observatory", Advances in High Energy Physics, 2013, 1-18.

Amato E (2014) "The Theory of Pulsar Wind Nebulae", Int. J. Mod. Phys. Conf. Ser., 28: 1460160-0 - 1460160-11.

Auger P, Ehrenfest P, Maze R, Daudin J, and Fréon RA (1939) "Extensive Cosmic-Ray Showers", Reviews of Modern Physics 288-29.

Bigas OB, Deligny O, Payet K and Elewyck VV (2009) "The propagation of ultra-high energy tau leptons and neutrinos while skimming the Earth", Nucl.Phys.Proc.Suppl. 190: 144-149.

Bluemer J, Engel R, and Hoerandel J (2009) "Cosmic Rays from the Knee to the Highest Energies", In: Prog.Part.Nucl.Phys. ,63 : 293–338.

Davidson N, Nanava G, Przedzinski T, Richter-Was E, Was Z (2012), "Universal Interface of TAUOLA", Computer Physics Communications, 183: 821-843.

Falkenburg B and Rhode W (2012) From Ultra Rays to Astroparticles, Springer, First Edition, Verlag.

Fukuda S (2003) "The Super-Kamiokande detector", Nuclear Instruments and Methods in Physics Research A, 501: 418–462.

Greisen K (1966) "End to the Cosmic-Ray Spectrum?", Physical Review Letters, 16: 748–750.

Griffiths D (2008) Introduction to Elementary Particles, Wiley, Second Revised Edition, Germany.

Hörandel JR (2003) "On the knee in the energy spectrum of cosmic rays", Astroparticle Physics,19: 193-220.

Karlsruhe Insitute of Technology, The KASCADE-Grande Experiment at KIT Campus North, https://www.ikp.kit.edu/corsika/, 27 January 2017.

Klapdor-Kleingrothaus HV (1997) K. Zuber, Teilchenastrophysik Teubner Studienbucher.

Matthews J (2005) "A Heitler model of extensive air showers", Astroparticle Physics 22: 387–397.

Mirabel IF and Rodríguez LF (1999) "Sources of relativistic jets in the Galaxy", Annual Review of Astronomy and Astrophysics, 37; 409.

Pierre Auger Collaboration, https://www.auger.org/index.php/cosmic-rays/detection, 27 January 2017.

Reynolds SP (2008) "Supernova Remnants at High Energy", Annual Review of Astronomy and Astrophysics ,46: 89-126

ROOT Data Analysis Framework, https://root.cern.ch/root-user-guides-and-manual, 27 January 2017.

The National Aeronautics and Space Administration, https://swift.gsfc.nasa.gov/, 27 January 2017

Ulrich H, Glasstetter R, Antoni T et al. (2004) "Energy spectrum and elemental composition of cosmic rays in the pev region", The European Physical Journal C - Particles and Fields,33: 944–946.

Yılmaz A (2011) Study of Prototype Detector For UHE Tau Neutrino Detection, Yüksek Lisans Tezi, AİBÜ Fen Bilimleri Enstitüsü, Bolu.

Zatsepin GT and Kuz'min VA (1966) "Upper Limit of the Spectrum of Cosmic Rays", JETP Letters, 4: 78–80.

APPENDICES

7. APPENDICIES

APPENDIX A

In Appendix A, mean values of showers that were pre-analyzed with respect to particle number on inclined plane and percentages of particle types will be detailed with tables. In the first part of appendix, mean values of particle number on inclined plane will be shown for nine showers that were produced with different shower energy, decay mode and decay length. In the second part of appendix, mean values of percentages that are gamma, electron-positron and muon-antimuon particles on inclined plane will be shown for nine showers that were produced with different shower energy, decay mode and decay length.

A1.1 : Number of Particles on Inclined Plane for π^- Showers

		Shower Energy (GeV) +/- Error									
		10^7 GeV	Error	$5x10^7$ GeV	Error	10^8 GeV	Error	$5x10^8$ GeV	Error	10^9 GeV	Error
Decay Length	3 km	2018952.55	482858.99	16786358.76	322131	5735580.33	1404937.14	64079047.49	34546265.85	99501150.92	48755264.45
	5 km	2843136.78	569270.06	16898740.86	2755066.14	14527343.21	5219532.37	104985105	27619053.31	156740014	62150208.03
	7 km	1785791.33	651204.78	11796062.01	2108237.17	11486154.34	3361945.27	94505307.35	31965836.66	93283353.3	29502433.45
	10 km	464407.22	117471.03	4482464.56	1359725.7	11854707.42	4930107.11	33131327.74	12903561.13	99203150.77	56636165.59

A1.1. In this table, mean values of particle numbers on inclined plane that produced by π^- showers with diffrent energy and decay length are written with errors. These mean values were gained by fitting function that f(x) = m for nine showers.

A1.2 : Number of Particles on Inclined Plane for $\pi^- \pi^0$ Showers

		Shower Energy (GeV) +/- Error									
		10^7 GeV	+/- Error	$5x10^7$ GeV	+/- Error	10^8 GeV	+/- Error	$5x10^8$ GeV	+/- Error	10^9 GeV	+/- Error
Decay Length	3 km	2443697	471339.84	11088062.43	3619103.24	20306809.98	530435.61	168268066.7	40004935.48	202372465.6	50843319.35
	5 km	4640992.22	865867.71	13618649.42	1983838.42	39331604.75	8203962.27	185395422.4	28723153.13	224079858.3	45130514.5
	7 km	2208362.56	630455.51	14105477	3657850.79	31565835.01	8471312.27	213432588.7	32156754.11	413437996.8	62054445.38
	10 km	1044100.78	330259.02	3283038.24	1036469.86	8651066.36	2854945.43	92500450.59	30733338.65	183645426.8	52059217.98

A1.2. In this table, mean values of particle numbers on inclined plane that produced by $\pi^- \pi^0$ showers with diffrent energy and decay length are written with errors. These mean values were gained by fitting function that f(x) = m for nine showers.

A1.3 : Number of Particles on Inclined Plane for $\pi^- \pi^0 \pi^0$ Showers

		Shower Energy (GeV) +/- Error									
		10^7 GeV	**+/- Error**	**$5x10^7$ GeV**	**+/- Error**	**10^8 GeV**	**+/- Error**	**$5x10^8$ GeV**	**+/- Error**	**10^9 GeV**	**+/- Error**
Decay Length	3 km	3030859.33	568585.47	10371203.1	3880061.98	33157679.3	7718840.55	115009035.3	43560609.51	191571197	77305303.56
	5 km	4852423.55	432615.29	28285675.53	4279799.08	51786262.87	6611690.57	201754070.7	27156255.61	288368761.2	47295080.31
	7 km	3707860.56	668567.99	22050527.9	4431407.52	47384873.89	6912751.78	169500223	23687330.91	387000763.1	45816082.11
	10 km	446111	104013.76	6383901.8	1798727.55	22852603.92	4934508.95	95261887.54	26003774.56	209993263	53893087.65

A1.3. In this table, mean values of particle numbers on inclined plane that produced by $\pi^- \pi^0 \pi^0$ showers with diffrent energy and decay length are written with errors. These mean values were gained by fitting function that f(x) = m for nine showers.

A1.4 : Number of Particles on Inclined Plane for $\pi^- \pi^- \pi^+$ Showers

		Shower Energy (GeV) +/- Error									
		10^7 GeV	**+/- Error**	**$5x10^7$ GeV**	**+/- Error**	**10^8 GeV**	**+/- Error**	**$5x10^8$ GeV**	**+/- Error**	**10^9 GeV**	**+/- Error**
Decay Length	3 km	3541859	810653.61	17720929.42	2657919.69	36156545.07	7840632.85	57733956.06	11707642.09	367806176.7	80680485.5
	5 km	4188058.67	496445.75	20962696.55	2483912.28	42148357.55	4482146.74	186674376.7	21633738.25	384185347.3	57849269.26
	7 km	1902677.11	364953.63	12885665.45	2868529.24	37276635.56	8246334.15	149818949.2	26403739.21	353168443.4	66553015.68
	10 km	649948.22	172881.62	5609862.45	1555956.18	19546533.58	2937541.3	56564731.67	18516682.98	158975644	49165948.59

A1.4. In this table, mean values of particle numbers on inclined plane that produced by $\pi^- \pi^- \pi^+$ showers with diffrent energy and decay length are written with errors. These mean values were gained by fitting function that f(x) = m for nine showers.

A2.1 : Particle Percentages on Inclined Plane for π^- Showers

		Shower Energy				
		10^7 GeV	$5x10^7$ GeV	10^8 GeV	$5x10^8$ GeV	10^9 GeV
Decay Length	3 km	64.8	66.1	63.1	64.2	64.6
	5 km	66.5	67.3	66.6	66.6	66.9
	7 km	67.3	69	63.1	68.3	68.6
	10 km	63.5	66	68.6	69.2	66.4

A2.1. In this table, mean values of gamma particle percentages on inclined plane that produced by π^- showers with diffrent energy and decay length are written with errors. These mean values were gained by fitting function that f(x) = m for nine showers.

		Shower Energy				
		10^7 GeV	$5x10^7$ GeV	10^8 GeV	$5x10^8$ GeV	10^9 GeV
Decay Length	3 km	32.7	31.4	33.2	32.9	33
	5 km	30.8	30.3	31.3	31.6	31.3
	7 km	26.5	28	33.2	29.2	29.2
	10 km	23.5	24.3	26.4	25.8	25.9

A2.2. In this table, mean values of electron-positron particle pair percentages on inclined plane that produced by π^- showers with diffrent energy and decay length are written with errors. These mean values were gained by fitting function that f(x) = m for nine showers.

		Shower Energy				
		10^7 GeV	$5x10^7$ GeV	10^8 GeV	$5x10^8$ GeV	10^9 GeV
Decay Length	3 km	1.7	1.8	1.6	1.4	1.4
	5 km	2.1	1.8	1.6	1.4	1.4
	7 km	5.4	2.5	2.3	2	1.8
	10 km	12	9	4.4	4.5	7.2

A2.3. In this table, mean values of muon-antimuon particle pair percentages on inclined plane that produced by π^- showers with diffrent energy and decay length are written with errors. These mean values were gained by fitting function that f(x) = m for nine showers.

A2.2 : Particle Percentages on Inclined Plane for $\pi^- \pi^0$ Showers

		Shower Energy				
		10^7 GeV	$5x10^7$ GeV	10^8 GeV	$5x10^8$ GeV	10^9 GeV
Decay Length	3 km	64.7	65.6	64.6	65.2	64.7
	5 km	67.9	66.9	67.6	67.1	65.5
	7 km	68.9	70.5	69.4	68.1	68.7
	10 km	70.4	69.2	68.6	71.4	69.3

A2.4. In this table, mean values of gamma particle percentages on inclined plane that produced by $\pi^- \pi^0$ showers with diffrent energy and decay length are written with errors. These mean values were gained by fitting function that f(x) = m for nine showers.

		Shower Energy				
		10^7 GeV	$5x10^7$ GeV	10^8 GeV	$5x10^8$ GeV	10^9 GeV
Decay Length	3 km	33.8	33.4	33.5	33	34.1
	5 km	30.8	32.3	31.3	32.2	33
	7 km	26.8	28.3	29	31.3	30.7
	10 km	24.9	24.2	24.9	27.1	26.8

A2.5. In this table, mean values of electron-positron particle pair percentages on inclined plane that produced by $\pi^- \pi^0$ showers with diffrent energy and decay length are written with errors. These mean values were gained by fitting function that f(x) = m for nine showers.

		Shower Energy				
		10^7 GeV	$5x10^7$ GeV	10^8 GeV	$5x10^8$ GeV	10^9 GeV
Decay Length	3 km	1	0.8	1.3	1.1	0.8
	5 km	1	0.6	0.9	0.5	1
	7 km	3.9	1	1.3	0.5	0.5
	10 km	4.2	6.1	6.1	1.4	3.6

A2.6. In this table, mean values of muon-antimuon particle pair percentages on inclined plane that produced by $\pi^- \pi^0$ showers with diffrent energy and decay length are written with errors. These mean values were gained by fitting function that f(x) = m for nine showers.

A2.3 : Particle Percentages on Inclined Plane for $\pi^- \pi^0 \pi^0$ Showers

		Shower Energy				
		10^7 GeV	$5x10^7$ GeV	10^8 GeV	$5x10^8$ GeV	10^9 GeV
Decay Length	3 km	65.4	63.8	65.3	63.8	64
	5 km	67.7	68.3	67.6	66.7	65.3
	7 km	69.9	70.2	69.7	70	69.8
	10 km	68.1	69.8	71.3	70.2	70.6

A2.7. In this table, mean values of gamma particle percentages on inclined plane that produced by $\pi^- \pi^0 \pi^0$ showers with diffrent energy and decay length are written with errors. These mean values were gained by fitting function that f(x) = m for nine showers.

		Shower Energy				
		10^7 GeV	$5x10^7$ GeV	10^8 GeV	$5x10^8$ GeV	10^9 GeV
Decay Length	3 km	33.2	33.9	33.3	33.9	34.1
	5 km	31.3	30.7	31.6	32.3	33.5
	7 km	28.2	28.6	29.4	28.9	29.2
	10 km	23.2	24.9	26.8	26.8	26.9

A2.8. In this table, mean values of electron-positron particle pair percentages on inclined plane that produced by $\pi^- \pi^0 \pi^0$ showers with diffrent energy and decay length are written with errors. These mean values were gained by fitting function that f(x) = m for nine showers.

		Shower Energy				
		10^7 GeV	$5x10^7$ GeV	10^8 GeV	$5x10^8$ GeV	10^9 GeV
Decay Length	3 km	0.9	1.4	0.9	1.4	1.2
	5 km	0.8	0.8	0.6	0.8	0.8
	7 km	1.6	1	0.7	0.9	0.8
	10 km	8.1	4.9	1.6	2.7	2.3

A2.9. In this table, mean values of muon-antimuon particle pair percentages on inclined plane that produced by $\pi^- \pi^0 \pi^0$ showers with diffrent energy and decay length are written with errors. These mean values were gained by fitting function that f(x) = m for nine showers.

A2.4 : Particle Percentages on Inclined Plane for $\pi^- \pi^- \pi^+$ Showers

		Shower Energy				
		10^7 GeV	$5x10^7$ GeV	10^8 GeV	$5x10^8$ GeV	10^9 GeV
Decay Length	3 km	65.2	64.3	64.8	62.5	64.9
	5 km	66.4	68.2	66.5	65.9	65.4
	7 km	68.1	68.4	68.1	68.3	68.9
	10 km	61.1	66.1	69.1	67.7	68.8

A2.10. In this table, mean values of gamma particle percentages on inclined plane that produced by $\pi^- \pi^- \pi^+$ showers with diffrent energy and decay length are written with errors. These mean values were gained by fitting function that f(x) = m for nine showers.

		Shower Energy				
		10^7 GeV	$5x10^7$ GeV	10^8 GeV	$5x10^8$ GeV	10^9 GeV
Decay Length	3 km	32	33.1	32.3	34.1	32.8
	5 km	30.7	29.2	31.3	32.4	33
	7 km	26.3	27.1	28.8	28.6	28.6
	10 km	23.1	24.5	26.9	25.4	25.9

A2.11. In this table, mean values of electron-positron particle pair percentages on inclined plane that produced by $\pi^- \pi^- \pi^+$ showers with diffrent energy and decay length are written with errors. These mean values were gained by fitting function that f(x) = m for nine showers.

		Shower Energy				
		10^7 GeV	$5x10^7$ GeV	10^8 GeV	$5x10^8$ GeV	10^9 GeV
Decay Length	3 km	2	1.7	1.9	2.1	1.5
	5 km	2.2	2.1	1.6	1.2	1.1
	7 km	4.9	3.9	2.8	2.6	2.1
	10 km	14.9	2.1	3.6	6.3	4.8

A2.12. In this table, mean values of muon-antimuon particle pair percentages on inclined plane that produced by $\pi^- \pi^- \pi^+$ showers with diffrent energy and decay length are written with errors. These mean values were gained by fitting function that f(x) = m for nine showers.

APPENDIX B

In Appendix B, mean values of detected particles by towers and its tiles that were analyzed with respect to the particle types will be detailed with tables. In the first part of appendix, mean values of detected particle number on by whole array will be shown for nine showers that were produced with different shower energy, decay mode and decay length. In the second part of appendix, mean values of detected particle, electron-positron, most fired central station will be shown for nine showers that were produced with different shower energy, decay mode and decay lengt

B1.1 : Detected Particles Information of Array for π^- Showers

		10^7 GeV			
		Electron-Positron	Error	Muon-Antimuon	Error
Decay Length	3 km	60.6	16.7	5.2	1.8
	5 km	91.2	17.7	6.9	1.1
	7 km	59.3	22.7	5.9	1.5
	10 km	16.9	4.5	3.3	0.8

B1.1. In this table, mean values of detected electron-positron and muon-antimuon particles by array for π^- showers that produced 10^7 GeV energy and decay length are written with errors. These mean values were gained by fitting function that f(x) = m for detected particles of nine showers.

		$5x10^7$ GeV			
		Electron-Positron	Error	Muon-Antimuon	Error
Decay Length	3 km	528.9	116.2	26.8	4.9
	5 km	540.7	92.3	32.3	5.5
	7 km	406.8	74	25.2	4.6
	10 km	149.1	46	17.4	4.1

B1.2. In this table, mean values of detected electron-positron and muon-antimuon particles by array for π^- showers that produced $5x10^7$ GeV energy and decay length are written with errors. These mean values were gained by fitting function that f(x) = m for detected particles of nine showers.

		10^8 GeV			
		Electron-Positron	Error	Muon-Antimuon	Error
Decay Length	3 km	153.6	41.7	15	3.3
	5 km	444	173.3	21.2	8.4
	7 km	389.2	112.5	9.4	2.6
	10 km	394.2	164.6	18.7	5.1

B1.3. In this table, mean values of detected electron-positron and muon-antimuon particles by array for π^- showers that produced 10^8 GeV energy and decay length are written with errors. These mean values were gained by fitting function that f(x) = m for detected particles of nine showers.

		$5x10^8$ GeV			
		Electron-Positron	Error	Muon-Antimuon	Error
Decay Length	3 km	1929.3	1087.1	103.1	48.3
	5 km	3107.1	813.4	137.6	33.6
	7 km	3307.3	1879.8	139.3	68.5
	10 km	1123.9	444.8	60	14.5

B1.4. In this table, mean values of detected electron-positron and muon-antimuon particles by array for π^- showers that produced $5x10^8$ GeV energy and decay length are written with errors. These mean values were gained by fitting function that f(x) = m for detected particles of nine showers.

		10^9 GeV			
		Electron-Positron	Error	Muon-Antimuon	Error
Decay Length	3 km	2727.3	1343.9	144.1	62.4
	5 km	4688.1	1834.9	198.4	73.2
	7 km	3146.8	1009.3	158.7	55.9
	10 km	3307.3	1879.8	139.3	68.5

B1.5. In this table, mean values of detected electron-positron and muon-antimuon particles by array for π^- showers that produced 10^9 GeV energy and decay length are written with errors. These mean values were gained by fitting function that f(x) = m for detected particles of nine showers.

B1.2 : Detected Particles Information of Array for $\pi^- \pi^0$ Showers

		10^7 GeV			
		Electron-Positron	Error	Muon-Antimuon	Error
Decay Length	3 km	58.2	12.4	3	0.5
	5 km	137.1	23.5	2.9	0.5
	7 km	76.9	21	2.9	0.8
	10 km	38.1	11.3	2.4	0.5

B1.6: In this table, mean values of detected electron-positron and muon-antimuon particles by array for $\pi^- \pi^0$ showers that produced 10^7 GeV energy and decay length are written with errors. These mean values were gained by fitting function that f(x) = m for detected particles of nine showers.

		$5x10^7$ GeV			
		Electron-Positron	**Error**	**Muon-Antimuon**	**Error**
Decay Length	3 km	296.3	102.3	9.4	1.8
	5 km	386.4	58.8	10.6	1.9
	7 km	480	112	9.2	3.9
	10 km	113	36.5	6.1	1.8

B1.7. In this table, mean values of detected electron-positron and muon-antimuon particles by array for $\pi^- \pi^0$ showers that produced $5x10^7$ GeV energy and decay length are written with errors. These mean values were gained by fitting function that f(x) = m for detected particles of nine showers.

		10^8 GeV			
		Electron-Positron	**Error**	**Muon-Antimuon**	**Error**
Decay Length	3 km	542.2	152	33	8.4
	5 km	1179.8	252.1	31.9	7.7
	7 km	1060.8	281.9	32.1	8.1
	10 km	290.2	96	19.1	5.7

B1.8: In this table, mean values of detected electron-positron and muon-antimuon particles by array for $\pi^- \pi^0$ showers that produced 10^8 GeV energy and decay length are written with errors. These mean values were gained by fitting function that f(x) = m for detected particles of nine showers.

		$5x10^8$ GeV			
		Electron-Positron	Error	Muon-Antimuon	Error
Decay Length	3 km	4735.9	1213.4	143.7	44.8
	5 km	5304	952.3	86.1	18.6
	7 km	6307.9	873.2	92	23.9
	10 km	3112.3	1010.2	54.4	7.3

B1.9. In this table, mean values of detected electron-positron and muon-antimuon particles by array for $\pi^- \pi^0$ showers that produced $5x10^8$ GeV energy and decay length are written with errors. These mean values were gained by fitting function that f(x) = m for detected particles of nine showers.

		10^9 GeV			
		Electron-Positron	Error	Muon-Antimuon	Error
Decay Length	3 km	5049.4	1451	126.9	31.5
	5 km	6229.6	1388.7	275.6	69.3
	7 km	12823.2	1742.5	188.3	37.7
	10 km	6163.3	1718.4	139.8	36.9

B1.10. In this table, mean values of detected electron-positron and muon-antimuon particles by array for $\pi^- \pi^0$ showers that produced 10^9 GeV energy and decay length are written with errors. These mean values were gained by fitting function that f(x) = m for detected particles of nine showers.

B1.3 : Detected Particles Information of Array for $\pi^- \pi^0 \pi^0$ Showers

		10^7 GeV			
		Electron-Positron	Error	Muon-Antimuon	Error
Decay Length	3 km	98.7	20.8	4.7	1.2
	5 km	142	11	3.7	0.7
	7 km	131.7	23.6	3.1	0.9
	10 km	14.3	3.2	2.4	0.7

B1.11. In this table, mean values of detected electron-positron and muon-antimuon particles by array for $\pi^- \pi^0 \pi^0$ showers that produced 10^7 GeV energy and decay length are written with errors. These mean values were gained by fitting function that f(x) = m for detected particles of nine showers.

		$5x10^7$ GeV			
		Electron-Positron	Error	Muon-Antimuon	Error
Decay Length	3 km	284	129.1	12.1	5.4
	5 km	871.8	126	20.6	4.7
	7 km	709.3	136.2	15.3	4
	10 km	214.1	62.2	12.3	3.3

B1.12: In this table, mean values of detected electron-positron and muon-antimuon particles by array for $\pi^- \pi^0 \pi^0$ showers that produced $5x10^7$ GeV energy and decay length are written with errors. These mean values were gained by fitting function that f(x) = m for detected particles of nine showers.

		10^8 GeV			
		Electron-Positron	Error	Muon-Antimuon	Error
Decay Length	3 km	931	246.8	24	5.4
	5 km	1547.9	224	34.9	8.8
	7 km	1545.9	210.9	26.2	5.4
	10 km	792.8	174.2	19.2	5

B1.13. In this table, mean values of detected electron-positron and muon-antimuon particles by array for $\pi^- \pi^0 \pi^0$ showers that produced 10^8 GeV energy and decay length are written with errors. These mean values were gained by fitting function that f(x) = m for detected particles of nine showers.

		$5x10^8$ GeV			
		Electron-Positron	Error	Muon-Antimuon	Error
Decay Length	3 km	2931.1	1207.3	111.3	24.1
	5 km	5808.1	858.7	170.6	32.5
	7 km	5660.3	766.2	130.4	20.5
	10 km	3277.9	893.3	100	18.9

B1.14. In this table, mean values of detected electron-positron and muon-antimuon particles by array for $\pi^- \pi^0 \pi^0$ showers that produced $5x10^8$ GeV energy and decay length are written with errors. These mean values were gained by fitting function that f(x) = m for detected particles of nine showers.

		10^9 GeV			
		Electron-Positron	**Error**	**Muon-Antimuon**	**Error**
Decay Length	3 km	4988.3	2218.7	169.3	40.9
	5 km	7627.3	1475.1	258.1	47.9
	7 km	12633.2	1439	231.4	43.8
	10 km	7117.3	1799.5	196.6	36.3

B1.15. In this table, mean values of detected electron-positron and muon-antimuon particles by array for $\pi^- \pi^0 \pi^0$ showers that produced 10^9 GeV energy and decay length are written with errors. These mean values were gained by fitting function that f(x) = m for detected particles of nine showers.

B1.4 : Detected Particles Information of Array for $\pi^- \pi^- \pi^+$ Showers

		10^7 GeV			
		Electron-Positron	**Error**	**Muon-Antimuon**	**Error**
Decay Length	3 km	108	26.8	6.3	1.3
	5 km	127.4	15.8	9.2	1.7
	7 km	66	12.8	7.2	0.9
	10 km	21.7	5.8	4.6	0.8

B1.16: In this table, mean values of detected electron-positron and muon-antimuon particles by array for $\pi^- \pi^- \pi^+$ showers that produced 10^7 GeV energy and decay length are written with errors. These mean values were gained by fitting function that f(x) = m for detected particles of nine showers.

		5x10^7 GeV			
		Electron-Positron	Error	Muon-Antimuon	Error
Decay Length	3 km	490	79.6	29.2	2.9
	5 km	689.3	79.9	37.3	2.4
	7 km	442.2	92.7	32.9	3.1
	10 km	21.8	1.8		

B1.17. In this table, mean values of detected electron-positron and muon-antimuon particles by array for $\pi^- \pi^- \pi^+$ showers that produced $5x10^7$ GeV energy and decay length are written with errors. These mean values were gained by fitting function that f(x) = m for detected particles of nine showers.

		10^8 GeV			
		Electron-Positron	Error	Muon-Antimuon	Error
Decay Length	3 km	1062.3	245.6	59.6	12.6
	5 km	1313.2	147.8	74.4	6.3
	7 km	1208.7	260.9	59.7	8
	10 km	675	99.5	47.6	5.8

B1.18. In this table, mean values of detected electron-positron and muon-antimuon particles by array for $\pi^- \pi^- \pi^+$ showers that produced 10^8 GeV energy and decay length are written with errors. These mean values were gained by fitting function that f(x) = m for detected particles of nine showers.

		$5x10^8$ GeV			
		Electron-Positron	Error	Muon-Antimuon	Error
Decay Length	3 km	1331.2	304.2	134.6	13.2
	5 km	5408.7	737.3	239.4	23.4
	7 km	4889.6	802.4	243	24.5
	10 km	1955	647.9	140.9	11.6

B1.14. In this table, mean values of detected electron-positron and muon-antimuon particles by array for $\pi^- \pi^- \pi^+$ showers that produced $5x10^8$ GeV energy and decay length are written with errors. These mean values were gained by fitting function that f(x) = m for detected particles of nine showers.

		10^9 GeV			
		Electron-Positron	Error	Muon-Antimuon	Error
Decay Length	3 km	10478	2594.4	513.2	65.8
	5 km	10667.8	1808.2	493.4	74.8
	7 km	10734.9	2258	483.3	79.5
	10 km	5373.1	1652.6	309.6	33.1

B1.15. In this table, mean values of detected electron-positron and muon-antimuon particles by array for $\pi^- \pi^- \pi^+$ showers that produced 10^9 GeV energy and decay length are written with errors. These mean values were gained by fitting function that f(x) = m for detected particles of nine showers.

B2.1 : Detected Particle of Most Fired Central Station for π^- Showers

		Shower Energy (GeV) +/- Error									
		10^7 GeV	Error	$5x10^7$ GeV	Error	10^8 GeV	Error	$5x10^8$ GeV	Error	10^9 GeV	Error
Decay Length	3 km	6.16	1.6	57.1	12.3	18.7	4.8	245.6	135.4	367.6	184.1
	5 km	9.7	2.5	60.9	10.9	51.7	17.4	395	105.6	588.8	236.8
	7 km	13	2.5	38.1	7.7	46.3	14.5	337.7	195.9	307.7	95.8
	10 km	2.7	0.6	11.9	4.6	53.1	23	101.6	52.4	337.7	196.8

B2.1. In this table, mean values of particle detected electron-positron numbers of most fired central stations for π^- showers that produced different energy and decay length are written with errors. These mean values were gained by fitting function that f(x) = m to most hitted central tiles of towers.

B2.2 : Detected Particle of Most Fired Central Station for $\pi^- \pi^0$ Showers

		Shower Energy (GeV) +/- Error									
		10^7 GeV	Error	$5x10^7$ GeV	Error	10^8 GeV	Error	$5x10^8$ GeV	Error	10^9 GeV	Error
Decay Length	3 km	9.7	1.9	46	15.1	75	19.4	649.1	159.3	755.2	201.2
	5 km	17	3.3	54.8	8.4	156.7	34.6	721.1	119.5	822.1	178.4
	7 km	13.2	3.1	54.1	15.1	117.8	35.1	847.1	133.6	1674	253.2
	10 km	5.6	1.9	11	3.4	30.1	9	329.9	126.7	695.4	223.6

B2.2. In this table, mean values of particle detected electron-positron numbers of most fired central stations for $\pi^- \pi^0$ showers that produced different energy and decay length are written with errors. These mean values were gained by fitting function that f(x) = m to most hitted central tiles of towers.

B2.3 : Detected Particle of Most Fired Central Station for $\pi^- \pi^0 \pi^0$ Showers

		Shower Energy (GeV) +/- Error									
		10^7 GeV	Error	$5x10^7$ GeV	Error	10^8 GeV	Error	$5x10^8$ GeV	Error	10^9 GeV	Error
Decay Length	3 km	14.6	2.6	35.9	14.4	127.6	30.9	420.1	169.7	717	313.3
	5 km	17.3	2.7	112	18.8	204	29	770.3	111.6	1063.7	191
	7 km	18.1	2.6	82.8	18.1	193.6	33.6	631.4	101.7	1518	201.3
	10 km	1.7	0.4	19.9	5.9	78.6	19	322.4	101	743.8	231.1

B2.3. In this table, mean values of particle detected electron-positron numbers of most fired central stations for $\pi^- \pi^0 \pi^0$ showers that produced different energy and decay length are written with errors. These mean values were gained by fitting function that f(x) = m to most hitted central tiles of towers.

B2.3 : Detected Particle of Most Fired Central Station for $\pi^- \pi^- \pi^+$ Showers

		Shower Energy (GeV) +/- Error									
		10^7 GeV	Error	$5x10^7$ GeV	Error	10^8 GeV	Error	$5x10^8$ GeV	Error	10^9 GeV	Error
Decay Length	3 km	12.3	3.6	67	10.8	130	29.1	199.4	44.3	1388	337.1
	5 km	15.1	3.2	76.3	12.7	166.3	18.3	692.1	84.9	1424.1	226.1
	7 km	5.4	1.3	37.7	11.7	131.3	34.7	516.7	107	1149.2	295.5
	10 km	3.5	1.5	15	5.2	54.8	13.4	160.4	64.8	490.2	191.7

B2.4. In this table, mean values of particle detected electron-positron numbers of most fired central stations for $\pi^- \pi^- \pi^+$ showers that produced different energy and decay length are written with errors. These mean values were gained by fitting function that f(x) = m to most hitted central tiles of towers.

8. CURRICULUM VITAE

Name SURNAME : Kaan Yüksel OYULMAZ
Place and Date of Birth : EMİNÖNÜ 09.07.1991
Universities
- Bachelor's Degree : Abant Izzet Baysal University
e-mail : kaan.oyulmaz@gmail.com
Address : Bahçelievler Mahallesi Çiğdem Sokak Çağdaş Sitesi Daire 9 BOLU/Merkez

List of Publications :

- **K. Y. OYULMAZ**, A. YILMAZ ve H.DENİZLİ, "Study of Angular Dependence of the Cosmic Ray Flux at 900 Meters Above Sea Level", 9th International Physics Conference of the Balkan Physical Union (BPU9), 2015
- **K. Y. OYULMAZ**, U.KESKİN, Ş. ATİK YILMAZ, A. YILMAZ VE H.DENİZLİ "CORSIKA Benzetim Programı Kullanılarak Çok Yüksek Enerjili Yukarı Yönlü Tau Nötrino Sağanakların Tespiti ve Tetiklemenin Belirlenmesi" Hızlandırıcı ve Algıç Fiziği Çalıştayı, 2016.
- Ş. ATİK YILMAZ, H. DENİZLİ, **K. Y. OYULMAZ**, U. KESKİN, A. YILMAZ "CORSIKA Benzetim Programı Kullanılarak Çok Yüksek Enerjili Yukarı Yönlü Tau Nötrino Sağanaklarının Çalışılması" Hızlandırıcı ve Algıç Fiziği Çalıştayı, 2016.
- **K. Y. OYULMAZ**, U.KESKİN VE H.DENİZLİ "Yukarı Yönlü Çok Yüksek Enerji Tau Nötrinonun Oluşturacağı Sağanakların Farklı Bozunma Mesafeleri ve Enerjierinde Özellikle π $\pi 0$ Bozunma Kanalı Kullanılarak Tespiti" XI. Ulusal Nükleer Bilimler ve Teknolojileri Kongresi ,2016

Awards :

- Poster Presentation Award:
  K. Y. OYULMAZ, U.KESKİN VE H.DENİZLİ "Yukarı Yönlü Çok Yüksek Enerji Tau Nötrinonun Oluşturacağı Sağanakların Farklı Bozunma Mesafeleri ve Enerjierinde Özellikle π $\pi 0$ Bozunma Kanalı Kullanılarak Tespiti" XI. Ulusal Nükleer Bilimler ve Teknolojileri Kongresi ,2016 (**3rd Place**)